Response and sensitivity of the nocturnal boundary layer over land to added longwave radiative forcing

R. T. McNider,[1] G. J. Steeneveld,[2] A. A. M. Holtslag,[2] R. A. Pielke Sr.,[3] S. Mackaro,[4] A. Pour-Biazar,[1] J. Walters,[5] U. Nair,[1] and J. Christy[1]

Received 13 February 2012; revised 25 May 2012; accepted 29 May 2012; published 18 July 2012.

[1] One of the most significant signals in the thermometer-observed temperature record since 1900 is the decrease in the diurnal temperature range over land, largely due to rising of the minimum temperatures. Generally, climate models have not well replicated this change in diurnal temperature range. Thus, the cause for night-time warming in the observed temperatures has been attributed to a variety of external causes. We take an alternative approach to examine the role that the internal dynamics of the stable nocturnal boundary layer (SNBL) may play in affecting the response and sensitivity of minimum temperatures to added downward longwave forcing. As indicated by previous nonlinear analyses of a truncated two-layer equation system, the SNBL can be very sensitive to changes in greenhouse gas forcing, surface roughness, heat capacity, and wind speed. A new single-column model growing out of these nonlinear studies is used to examine the SNBL. Specifically, budget analyses of the model are provided that evaluate the response of the boundary layer to forcing and sensitivity to mixing formulations. Based on these model analyses, it is likely that part of the observed long-term increase in minimum temperature is reflecting a redistribution of heat by changes in turbulence and not by an accumulation of heat in the boundary layer. Because of the sensitivity of the shelter level temperature to parameters and forcing, especially to uncertain turbulence parameterization in the SNBL, there should be caution about the use of minimum temperatures as a diagnostic global warming metric in either observations or models.

Citation: McNider, R. T., G. J. Steeneveld, A. A. M. Holtslag, R. A. Pielke Sr., S. Mackaro, A. Pour-Biazar, J. Walters, U. Nair, and J. Christy (2012), Response and sensitivity of the nocturnal boundary layer over land to added longwave radiative forcing, *J. Geophys. Res.*, *117*, D14106, doi:10.1029/2012JD017578.

1. Background

[2] The present paper explores two issues related to the stable nocturnal boundary layer that have recently received attention in the literature. These issues are discussed below.

1.1. Observed Diurnal Asymmetry in Warming

[3] Observations have been a key factor in the validation of model projections of heat accumulation in the atmosphere due to atmospheric greenhouse forcing. Surface observations of global temperature have shown overall warming since the middle of the 19th century, which is consistent with the expectation that heat is accumulating in the atmosphere. There is, however, a curious aspect of the surface data over land in that there is a strong asymmetry in warming between day and night through most of the temperature record [*Karl et al.*, 1993; *Vose et al.*, 2005]. Generally, the most used surface data sets (Goddard Institute for Space Studies [*Hansen et al.*, 1999] and East Anglia/Hadley Center [*Brohan et al.*, 2006]) only include one temperature for the day, T_{mean}, which is the daily average of the maximum temperature, $T_{\max}$, and minimum temperature, $T_{\min}$. However, data sets such as the NOAA Global Historical Network [*Peterson and Vose*, 1997; *Easterling et al.*, 1997], which partition the global temperature into minimum and maximum temperatures for a day show that nearly 2/3 of the warming over land has occurred in minimum temperatures (see Figure 1). While *Vose et al.* [2005] have shown that the differential warming has decreased significantly since 1979, the number of stations in the Global Historical Climate Network (GHCN) since 1979 has also decreased substantially with very little coverage in the developing world. Analyses of East Africa temperatures [*Christy et al.*, 2009] in fact show increasing differences in day and night warming since 1979.

[1]Earth System Science Center, University of Alabama in Huntsville, Huntsville, Alabama, USA.
[2]Meteorology and Air Quality Section, Wageningen University, Wageningen, Netherlands.
[3]CIRES and ATOC, University of Colorado Boulder, Boulder, Colorado, USA.
[4]Vaisala Inc., Boulder, Colorado, USA.
[5]Southern Company, Birmingham, Alabama, USA.

Corresponding author: R. T. McNider, Earth System Science Center, University of Alabama in Huntsville, Huntsville, AL, USA. (mcnider@nsstc.uah.edu)

0148-0227/12/2012JD017578

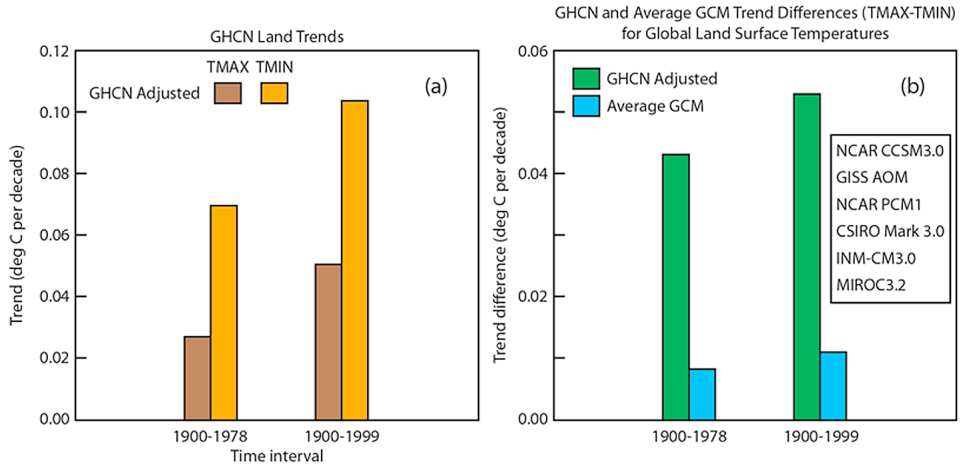

Figure 1. (a) Observed land surface trends from NOAA's Global Historical Climate Network (GHCN) [see *Vose et al.*, 2005]. (b) Difference in trends in minimum and maximum temperatures from an average of six global models from the Climate Model Intercomparison Project 3 (CMIP3) compared to the GHCN data set. The six models (their CMIP acronym) are listed above and in Table 1.

[4] Despite the fact that this diurnal asymmetry in warming is one of the most significant signals in the historical data, climate models including greenhouse gas forcing have in general not captured the magnitude of this asymmetry. In a sampling of six climate models that had minimum and maximum temperatures in the World Climate Research Programme's (WCRP's) Coupled Model Intercomparison Project phase 3 (CMIP3) multimodel data set [*Meehl et al.*, 2007] (see Table 1), we found the difference in trend between T_{max} and T_{min} to only be 20% of the trend difference in the GHCN data set (see Figure 1). This is almost identical to what *Zhou et al.* [2010] found - that the simulated diurnal temperature range trend was only 22% of the observed trend. This is also consistent with older findings of *Cao et al.* [1992], which indicated little skill in GCM diurnal trends and *Stone and Weaver* [2003] who found only about 30% of the trend difference in the GCM simulations. *Zhou et al.* [2010] provide a comprehensive review of the simulated and observed Diurnal Temperature Range (DTR) trends. Since climate models with greenhouse gas forcing have understated the trend in the DTR, investigators have attributed the change to a variety of causes not well represented in climate models such as increased cloud cover, jet contrails, or changes in surface characteristics such as land cover and land use [*Dai et al.*, 1999; *Durre and Wallace*, 2001; *Travis et al.*, 2004; *Christy et al.*, 2006]. Most recently, *Zhou et al.* [2010] concluded "The much larger observed decrease in DTR suggests the possibility of additional regional effects of anthropogenic forcing that the models cannot realistically simulate, likely connected to changes in cloud cover, precipitation, and soil moisture."

[5] *Walters et al.* [2007] took an alternative approach and examined the role nonlinear boundary layer dynamics [*Van de Wiel et al.*, 2002a, 2002b; *ReVelle*, 1993; *McNider et al.*, 1995; *Mahrt*, 1999; *Acevedo and Fitzjarrald*, 2001] might play in the warming of the nocturnal boundary layer (SNBL). Using numerical continuation [*Doedel et al.*, 1991] for a simple two-layer model, *Walters et al.* [2007] found that slight changes in incoming longwave radiation can destabilize the SNBL. This in turn mixes warm air to the surface leading to warming in the surface temperature due to a redistribution of heat. This was referred to as a positive climate feedback in that the surface warming due to the added greenhouse gas forcing was amplified by this redistribution of heat. *Walters et al.* [2007] further proposed that coarse-grid global climate models (GCMs) may not have the resolution or the type of turbulent closures that can capture this nonlinear behavior. While the other factors (e.g., contrails, aerosols, surface moisture) not well incorporated in models may be in play, *Walters et al.* [2007] concluded that sensitive SNBL behavior and the relatively crude resolution of the SNBL in GCMs may partly explain the general lack of fidelity in GCMs in replicating the magnitude of the historical observed asymmetry. *Durre and Wallace* [2001] and

Table 1. List of Climate Models Used to Calculate Model DTR Trends in Figure 1

Institution	Country	Model
National Center for Atmospheric Research	USA	CCSM3
CSIRO Atmospheric Research	Australia	CSIRO-Mk3.0
NASA / Goddard Institute for Space	USA	GISS-AOM
Institute for Numerical Mathematics	Russia	INM-CM3.0
Center for Climate System Research (The University of Tokyo), National Institute for Environmental Studies, and Frontier Research Center for Global Change (JAMSTEC)	Japan	MIROC3.2
National Center for Atmospheric Research	USA	PCM

Pielke et al. [2007] had also alluded to complexities of SNBL in impacting the asymmetry.

[6] The *Walters et al.* [2007] analysis, while including surface and atmospheric parameterizations close to the form used in mesoscale and global scale models, was carried out within the context of a truncated two-layer system. Also, the nonlinear analysis neglected clear air radiative cooling. In the present paper, we re-examine the findings of *Walters et al.* [2007] using a more complete multilayer model with full radiative forcing.

1.2. Nocturnal Warming Related to Wind Speed

[7] Using the historical surface data set, *Parker* [2004, 2006] examined whether sites might have an urban warming bias. Parker's fingerprint test was that the strength of the nighttime urban heat island (UHI) was hypothesized to be inversely dependent on wind speed. This premise seems largely sound based on many UHI studies [e.g., *Johnson et al.*, 1991]. Since Parker found no dependence on wind speed of trends in his data, he concluded that the warming in the data was not due to the UHI effect. He further concluded that the warming in the record must be due to greenhouse gas (GHG) increases.

[8] *Pielke and Matsui* [2005] (hereafter referred to as PM05) in a follow up to the Parker study, used a simple analytical model of the SNBL developed by *Stull* [1983] to examine if long-term climate trends of surface air temperature should not be expected to have the same trends for light wind and stronger wind nights, even if the trends of the nocturnal boundary layer heat flux divergence were the same. They presented an idealized analysis to illustrate why temperature values at specific levels should depend on wind speed, and with the same boundary layer heat content change, trends in temperature should be expected to be different at every height near the surface when the winds are light, as well as different between light wind and stronger wind nights. Thus, PM05 questioned whether Parker's finding that warming was due to GHG forcing was correct since GHG forcing in their model would also have an inverse dependence on wind speed, and this information was not found in the data.

[9] In employing the analytical model of Stull, PM05 added the GHG forcing as a constant perturbation independent of wind speed. Recently, *Steeneveld et al.* [2011] revisited the PM05 study using a much more complete state-of-the-art boundary layer model. Counter to the PM05 results, they showed in the more complete model that added GHG forcing produced a temperature perturbation that was largely independent of wind speed. Thus, *Steeneveld et al.* [2011] concluded that Parker's implicit assertion that GHG trends were independent of wind speed were consistent with the more complete model. However, they noted that a second conclusion of PM05, that greenhouse gas forcing was strongly dependent on height in the SNBL, was supported in the more complete model.

[10] The *Steeneveld et al.* [2011] studies dealt with a limited parameter space of the SNBL, especially in regard to surface roughness and land surface coupling. It also did not present details of the response and behavior of the SNBL to the added forcing. In the present paper, we explore the response and partitioning of the added GHG energy in much greater detail and in a broader parameter space.

1.3. Structure of the Paper

[11] Because the present paper is relatively detailed, here we provide a brief discussion of the structure of the paper and preliminary findings to provide a context for the details which follow. Section 2 provides a detailed description of the modeling tools employed in the paper which is a full single multilayer column and compares it to the simpler two layer models of *McNider et al.* [1995] and *Walters et al.* [2007] used in the dynamical studies. It also makes comparison and evaluation to other models.

[12] Section 3 compares the behavior of the full column model to the dynamical analyses of the two layer model for the case when clear air radiative forcing is ignored as in *Walters et al.* [2007]. The simple two layer model had shown an abrupt transition between a cold weak wind state in which the first atmospheric layer is turbulently connected to the surface and a warm windy state in which the first atmosphere is turbulent connected to the outer atmospheric layer. The results show that in the full column model the general behavior of the simpler model is retained, however, the transition between the two stable attracting states is muted in that the transition between the two states is not as abrupt. The full column model also shows the existence of a third state in which at low wind speeds turbulence is suppressed to the point that the atmosphere becomes completely disconnected from the surface and remains relatively warm. These states are discussed in comparison to previous studies about the collapse of turbulence by *Derbyshire* [1999], *Holtslag et al.* [2007] and *Basu et al*. [2008]. Section 3 also examines the response of the column model stable boundary layer to added longwave forcing and compares it to the simple two layer results reported by *Walters et al.* [2007]. The column model results shows that in certain parameter spaces the shelter level temperature can be quite sensitive to the added downward radiation with substantial warming occurring although the magnitude was less than in the two layer model.

[13] Section 4 goes into the details of the physics of the SNBL subjected to added forcing by developing energy budgets for the atmosphere, ground and losses to the system in order to determine where the added energy ends up being partitioned in the system. The most important finding is that the column model supports the conjecture of *Walters et al.* [2007] that the shelter level warming is largely due to a redistribution of heat as the SNBL grows. In effect the added energy destabilizes slightly the SNBL causing a growth of the boundary layer which then entrains warmer air to the surface.

[14] Section 5 relaxes the assumption of no clear air radiative forcing in the column model. A full modern radiative transfer scheme is employed. The clear air radiative forcing deepened and smoothed the temperature profile and the transition between the different coupled states was more muted. However, the budget calculations showed that the warming at shelter level was still largely due to a redistribution of heat due to growth of the boundary layer.

[15] Section 6 examines the dependence of temperature change at shelter level on wind speed due to added longwave forcing and thus revisits the works of *Parker* [2004], *Pielke and Matsui* [2005] and *Steeneveld et al.* [2011] using the present model and detailed budget calculations. The results from the present modeling study confirm the results

of *Steeneveld et al.* [2011] that the temperature response is largely independent of wind speed contrary to the *Pielke and Matsui* [2005] analysis that the response should be inversely proportional to wind speed. The present modeling study shows that the magnitude of the shelter level response is due a redistribution of heat by turbulence and the response is not totally controlled by the added surface fluxes as suggested by *Steeneveld et al.* [2011].

2. Model Description and Evaluation

2.1. Model Characteristics

[16] The basic model employed in the present study is an extension of the truncated two-layer model used in a series of nonlinear analysis studies [e.g., *McNider et al.*, 1995; *Shi et al.*, 2005; *Walters et al.*, 2007] exploring the behavior and parameter dependence of the stable boundary layer. While simple, the nonlinear analysis models retained a fairly realistic ground surface and interaction with the atmosphere. The relative simplicity of the model allowed for use of powerful nonlinear analysis tools developed by the mathematical community [*Doedel et al.*, 1991; *Friedman and Qiu*, 2008]. With these tools, parameter dependence (e.g., geostrophic wind, roughness, surface heat capacity) could be explored through construction of bifurcation diagrams. It also allowed calculation of eigenvalues, so the stability and character (smooth or oscillating) of the solutions could be determined. However, in the history of nonlinear analysis it is sometimes found that exotic dynamical behavior found in simple representations of reality are not carried forward as explicitly in more complete representations [*Seydel*, 1988]. For example, *Lorenz* [1995], in a discussion on atmospheric predictability, noted that "prediction errors in chaotic systems tend to amplify less rapidly on average as the system gets larger." The additional degrees of freedom tend to smooth or dampen the rate at which individual perturbed states depart over time.

[17] The more complete model presented in this paper is a specific model for the dry stable/neutral boundary layer. It is limited since it does not include daytime unstable boundary layer or moist processes other than initial water vapor profiles. It is also limited to simple initialization. Thus, it is not a complete boundary layer model as described by [*André et al.*, 1978; *McNider and Pielke*, 1981; *Duynkerke*, 1991; *Steeneveld et al.*, 2006]. However, it serves as a transition in relaxing the simplifications of the nonlinear analysis models by moving from a two-layer limited domain model with no clear air radiative forcing to a high resolution multilayer model with explicit radiative forcing. As discussed below, its numerical schemes and grid structure were selected to keep numerical diffusion to an absolute minimum at the expense of numerical efficiency. Also, engineering specifications that impose minimum mixing such as minimum diffusion coefficients and minimum values of surface stress were taken almost to zero. The model, as constructed, is intended to examine the sensitivity and behavior of the SNBL to explicit mixing formulations. Models are not perfect and engineering fixes are often needed to make models relevant to the real atmosphere [*Delage*, 1997; *Derbyshire*, 1999]. Thus, the present model may not be appropriate for full weather forecast applications or global climate simulations. However, in the present paper, we do make comparisons to another more complete SNBL model [*Steeneveld et al.*, 2006].

2.2. Model Description

[18] For the analyses herein, we consider a simple, one-dimensional (single column) model $u = u(z, t)$, $v = v(z, t)$, $\theta = \theta(z, t)$, and $q(z,t)$ [*Stull*, 1988] that closely represents the type columns embedded within weather forecast and air pollution models.

$$\frac{\partial u}{\partial t} = f_{co}(v - v_G) + \frac{\partial}{\partial z}\left(K_m(z, u_z, v_z, \theta_z)\frac{\partial u}{\partial z}\right), \tag{1}$$

$$\frac{\partial v}{\partial t} = f_{co}(u_G - u) + \frac{\partial}{\partial z}\left(K_m(z, u_z, v_z, \theta_z)\frac{\partial v}{\partial z}\right), \tag{2}$$

$$\frac{\partial \theta}{\partial t} = R_c(\theta) + \frac{\partial}{\partial z}\left(K_h(z, u_z, v_z, \theta_z)\frac{\partial \theta}{\partial z}\right., \tag{3}$$

$$\frac{\partial q}{\partial t} = \frac{\partial}{\partial z}\left(K_h(z, u_z, v_z, \theta_z)\frac{\partial q}{\partial z}\right., \tag{4}$$

[19] In equation (3), R_c is the clear-air radiative cooling rate for the air temperature, and in the original nonlinear analyses, was taken to be zero. The atmospheric equations were coupled with a prognostic surface energy budget equation for a simple slab with a bulk heat capacity $C_b = \rho_s c_s \Delta h$

$$\frac{dT_g(t)}{dt} = \frac{1}{C_b}\left(I_1|_{z=z_0} - \sigma T_g^4(t) - H_0|_{z=z_0}\right) - \rho_s c_s k_s \left(T_g(t) - T_m\right)\Delta h^{-1} \tag{5}$$

where ρ_s, c_s and k_s represent the soil density, soil specific heat capacity, and soil diffusivity. The term Δh represents the depth of the slab. A surface emissivity of 1.0 is assumed. This system is a bit more complex than the coupled system described by *Derbyshire* [1999] and involves physically based parameters but its simplicity, as with Derbyshire's system, makes analysis simpler than full coupled complex vegetative, water, and ground systems. Similar single column forms have been used by various investigators including *Blackadar* [1979], *Garratt and Brost* [1981], and *Steeneveld et al.* [2010].

[20] In the original nonlinear analysis studies, the longwave back radiation from the atmosphere (I_1) in equation (5) was simply parameterized following *Staley and Jurica* [1972] as

$$I_1 \equiv I_1\left(T_1\right)|_{z=z_0} = 0.67\sigma(1670Q_a)^{0.08}T_1^4|_{z=z_0} \tag{6}$$

where T_1 is the air temperature at the first model level, Q_a is the near surface specific humidity (in the column model this is the first level humidity), 0.67 and 1670 are dimensionless constants. Note I_1 is the downward longwave radiation at the surface while R_c in equation (3) is the longwave flux divergence.

[21] In the present study, we employ a full state-of-the-art Delta four-stream radiative transfer scheme of *Fu and Liou*

[1993] implemented following [*Wang and Christopher*, 2006; *Wang et al.*, 2006] for the clear air radiative forcing R_c and for the downward radiation, I_1, in equation (6).

[22] In equation (5), H_0 is the sensible heat flux by turbulence, and the last term in equation (5) is the heat flux from the slab to the substrate [*Blackadar*, 1979] of temperature T_m. The kinematic sensible heat flux is defined from similarity theory as $H_o = -u_*\theta_*$ where u_* and θ_* represent the friction velocity and friction temperature respectively. Note latent heat fluxes from the surface are ignored.

[23] As noted by *McNider et al.* [1995], the nonlinearity in the equations enters through the heat flux and first order closure turbulent diffusion terms, where

$$K_m = K_m(z, u_z, v_z, \theta_z) \text{ and } K_h = K_h(z, u_z, v_z, \theta_z)$$

are the exchange coefficients for momentum and heat, which in the absence of geostrophic wind shear are functions of the space variable z and the partial derivatives:

$$u_z = \partial u(z,t)/\partial z, \qquad v_z = \partial v(z,t)/\partial z, \qquad \theta_z = \partial\theta(z,t)/\partial z.$$

[24] The diffusion coefficients and surface fluxes are constructed in the form of these stability functions dependent on the gradient Richardson Number (Ri).

$$K_m = f_m(Ri) l^2 \mathrm{s}, \qquad K_h = f_h(Ri) l^2 \mathrm{s}.$$

[25] The length scale l near the surface and vertical wind shear s are defined as

$$l = \kappa z, \quad \mathrm{s} \equiv \mathrm{s}(u_z, v_z) = \sqrt{u_z^2 + v_z^2}.$$

[26] At the first model level, a flux condition is imposed so

$$\frac{du_1}{dt} = f_{co}(v_1 - v_G) + \frac{1}{z_{3/2} - z_{1/2}}\left(\frac{K_{m,3/2}(u_2 - u_1)}{z_2 - z_1} - u_*^2\cos(\psi)\right), \tag{7}$$

$$\frac{dv_1}{dt} = f_{co}(u_G - u_1) + \frac{1}{z_{3/2} - z_{1/2}}\left(\frac{K_{m,3/2}(v_2 - v_1)}{z_2 - z_1} - u_*^2\sin(\psi)\right), \tag{8}$$

$$\frac{d\theta_1}{dt} = \frac{1}{z_{3/2} - z_{1/2}}\left(\frac{K_{h,3/2}(\theta_2 - \theta_1)}{z_2 - z_1} - u_*\theta_*\right), \tag{9}$$

$$\frac{dq_1}{dt} = \frac{1}{z_{3/2} - z_{1/2}}\left(\frac{K_{h,3/2}(q_2 - q_1)}{z_2 - z_1} - u_* q_*\right), \tag{10}$$

where u_* and θ_* are the friction velocity, friction temperature, and friction humidity following *England and McNider* [1995] given by:

$$u_* = \frac{\kappa\sqrt{f_m(Ri_{1/2})}\sqrt{u_1^2 + v_1^2}}{\ln(z_1/z_0)},$$

$$\theta_* = \frac{\kappa(\theta_1 - \theta_a) f_h(Ri_{1/2})}{\sqrt{f_m(Ri_{1/2})}\ln(z_1/z_0)},$$

$$q_* = \frac{\kappa(q_1 - q_a) f_h(Ri_{1/2})}{\sqrt{f_m(Ri_{1/2})}\ln(z_1/z_0)},$$

and

$$\psi = \arctan(v_1/u_1),$$

$$z_{1/2} = z_1/2,$$

$$z_{3/2} = (z_1 + z_2)/2,$$

$$K_{m,3/2} = f_m(Ri_{3/2})\, l_{3/2}^2 \mathrm{s}_{3/2},$$

$$K_{h,3/2} = f_h(Ri_{3/2})\, l_{3/2}^2 \mathrm{s}_{3/2},$$

$$Ri_{3/2} = \frac{g}{\theta_A}\frac{(z_2 - z_1)(\theta_2 - \theta_1)}{(u_2 - u_1)^2 + (v_2 - v_1)^2},$$

$$Ri_{1/2} = \frac{g}{\theta_A}\sqrt{z_0 z_1}\ln\left(\frac{z_1}{z_0}\right)\frac{\theta_1 - \theta_a}{u_1^2 + v_1^2},$$

$$l_{3/2} = \kappa z_{3/2},$$

$$\mathrm{s}_{3/2} = \frac{\sqrt{(u_2 - u_1)^2 + (v_2 - v_1)^2}}{z_2 - z_1}.$$

[27] Note that the first level equations, when coupled to the surface energy budget equation with $\theta_a = T_g$ and a fixed (constant) layer aloft, are equivalent to the dynamical analysis set employed in *McNider et al.* [1995] and *Walters et al.* [2007]. In the present single column model, we deviate from using T_g in the surface flux as in the dynamical system by defining a true skin temperature T_R then compute an aerodynamic temperature, θ_a, for use in the sensible heat flux terms. The skin temperature, T_R, is calculated from a surface energy equation (11) derived from (5) that is infinitely thin and thus has no thermal inertia (zero heat capacity). This follows the formulation of *Pielke and Mahrer* [1975] and *McNider and Pielke* [1981] and more recently the NOAH land surface model [*Ek et al.*, 2003] and the ECMWF [*Viterbo and Beljaars*, 1995]. The skin temperature, T_R, is found by root finding of the algebraic equation for the surface energy balance of the infinitely thin surface

$$I_1\big|_{z=z_0} - \sigma T_R{}^4 - \rho c_p u_*\theta_* - \rho_s c_s k_s (T_R - T_G)\Delta h_{eff}{}^{-1} = 0. \tag{11}$$

[28] *Van de Wiel et al.* [2002b] and *Steeneveld et al.* [2006] noted that the fast response of the surface temperature is important in simulating the SNBL and in their model

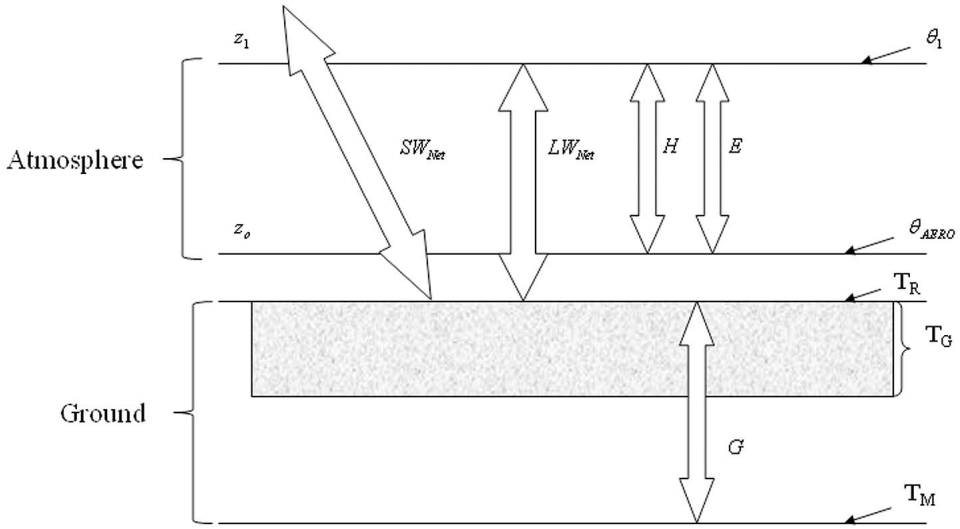

Figure 2. Schematic of ground surface and atmosphere interaction [from *Mackaro et al.*, 2011].

employed a vegetative mulch layer with small heat capacity. We employ the skin temperature for that purpose.

[29] While radiometers from both satellite and on in situ platforms have made radiating skin temperatures a measurable quantity, previous work [*Sun and Mahrt*, 1995] has indicated that skin temperatures cannot be directly used in traditional similarity forms for deducing fluxes. There are several alternatives as discussed by Sun and Mahrt. We employ an empirical formula to relate the skin temperature to the temperature at model roughness height, z_o and thus provide an aerodynamic temperature. Other modelers [e.g., *Steeneveld et al.*, 2006] adjust the roughness height for heat transfer, i.e., $z_{oH} = z_o/10$.

[30] To obtain an aerodynamic temperature from information available in the model, we employ a method suggested by *Zilitinkevich* [1970] and *Deardorff* [1972] to relate the temperature at z_o to the model skin temperature;

$$\theta_a = \theta_{Zo} = T_R + 0.0962\left(\theta_*/k\right)\left(u_* z_o/\nu\right)^{0.45} \qquad (12)$$

where ν is the kinematic viscosity of air. This technique has also been employed by *Pielke and Mahrer* [1975] and *McNider et al.* [1994].

[31] In summary, four temperatures are used to construct the lower flux boundary condition for the atmosphere: (1) an aerodynamic temperature- θ_a, (2) a skin temperature- T_R, (3) an active ground temperature (slab temperature) - T_g, and (4) a constant substrate temperature -T_m. Figure 2 provides a schematic of these surface and atmospheric temperatures.

[32] The present model differs from some boundary layer models in that the model does not explicitly employ Monin-Obukhov (M-O) similarity through the use of $\underline{z/L}$ as the stability parameter (where L is the Obukhov Length) [see *Stull*, 1988]. Rather, Richardson number dependent stability functions are employed [*Louis*, 1979; *England and McNider*, 1995]. The diffusion coefficients and surface fluxes are constructed in the form of these stability functions dependent on the gradient Richardson Number (Ri).

$$K_m = f_m(Ri) l^2 \mathrm{s}, \qquad K_h = f_h(Ri) l^2 \mathrm{s}.$$

[33] As noted by *England and McNider* [1995], the normal use of M-O theory requires an iteration since the velocity and temperature scales, u_* and θ_* are recursively dependent on L, which is dependent on u_* and θ_*. In carrying out the nonlinear analysis studies using nonlinear analysis tools [e.g., *Doedel et al.*, 1991] such recursive forms are invalid. Thus, there is a need for an explicit form. *Blackadar* [1979] had also formed a non-recursive closure based on shear functions. However, the stability function which Blackadar algebraically derived was a linear form:

$$f_m(Ri) = f_h(Ri) = \begin{cases} (1 - Ri/Ri_c), & \text{if } 0 \le Ri \le Ri_c, \\ 0, & \text{if } Ri \ge Ri_c. \end{cases}$$

[34] Again, from a nonlinear analysis perspective, the Blackadar form was not desirable in that it was discontinuous at $Ri = Ri_c$. *England and McNider* [1995] showed that the Monin-Obukhov profiles developed by *Businger et al.* [1971] and others can best be approximated as quadratic stability functions f_m and f_h (in terms of the Richardson-number formulations). The quadratic stability functions f_m and f_h (namely, the Richardson-number formulations) are given by *England and McNider* [1995] as

$$f_m(Ri) = f_h(Ri) = \begin{cases} (1 - Ri/Ri_c)^2, & \text{if } 0 \le Ri \le Ri_c, \\ 0, & \text{if } Ri \ge Ri_c. \end{cases} \qquad (13)$$

with $\mathrm{Ri}_c = 0.25$ used in the present study.

[35] This form is continuous both at $Ri = Ri_c$ and at neutrality, $Ri = 0$. The lack of iteration and singular dependence on Ri means that different forms of mixing that can be collapsed to the Ri form can be intercompared. Figure 3 provides a range of different stability functions that have been

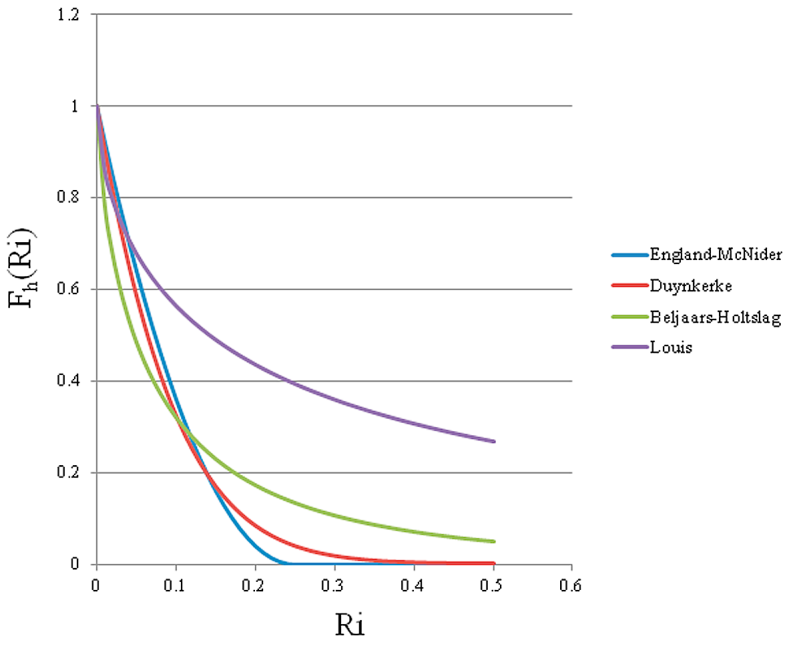

Figure 3. Stability functions used in the present paper. Ri is the gradient Richardson number. See *England and McNider* [1995], *Duynkerke* [1991], *Beljaars and Holtslag* [1991], and *Louis* [1979]. Duynkerke, Beljaars and Holtslag, and Louis represent curve fits to the original parameterization. See also *Van de Wiel et al.* [2002a].

employed in the literature for studies of the SNBL and that will be used in the present paper. These forms have been classified as short-tail and long-tail forms. The *Duynkerke* [1991] and *England and McNider* [1995] forms to be used later are referred to as short-tail forms in that there is little mixing beyond a critical Richardson Number of ~0.25. These forms, as noted by *Delage* [1997], seem to represent best the fundamental behavior of observations of idealized SNBLs. However, as discussed by *Delage* [1997], application of these forms in coarse grid and operational models seemed to provide too little mixing so that model performance was compromised [*Beljaars and Holtslag*, 1991; *Van de Wiel et al.*, 2002a]. *Delage* [1997] argued following *Mahrt* [1987] that areal averages such as grid averages in LES models yielded larger Ri than specific grid point data. Thus, longer-tailed functions of the Beljaars-Holtslag [*Beljaars and Holtslag*, 1991] and *Louis* [1979] forms have been utilized in weather forecast models and GCMs [*Holtslag and Boville*, 1993; *Viterbo and Beljaars*, 1995; *Viterbo et al.*, 1999].

2.3. Model Numerics

[36] Most standalone column models in use today [*Duynkerke*, 1991] or embedded within mesoscale models [*Pielke and Mahrer*, 1975; *McNider and Pielke*, 1981] utilize implicit or semi-implicit schemes such as the Crank-Nicholson scheme to solve the diffusion operator. These remove the Fourier condition for linear stability ($K\Delta t/(\Delta z)^2 \leq 1/2$), so much larger time steps can be taken. However, these implicit schemes can also provide spurious changes of small-scale features ($2\Delta z$ and $4\Delta z$ waves) [*Pielke*, 1984]. Since we are trying to minimize any mixing not explicitly arising from the turbulent parameterization, the present model reverted back to an explicit scheme. Thus, to maintain stability, small time steps were required of generally less than 0.2 s.

[37] As with most atmospheric models, we employ operator splitting in solving the column model by separating the land surface calculations from the diffusion step. While pragmatic, this operator splitting means that true mathematical coupling is not retained. Most column models employ a simple Euler step to solve the prognostic equation for the ground temperature (equation (5)). However, while the Euler step may be stable for large time steps, significant loss of accuracy can occur if large time steps are used since the terms such as H_0 and the outgoing radiation can vary rapidly over longer time steps. In our case, the very small time steps required for the diffusion operator ensures relatively high accuracy in the Euler step of the prognostic slab equation. However, in carrying out the energy budget calculations, we found that the very small time steps employed were producing a loss of significance in the Euler step. We found that even though the flux terms on the right-hand side of equation (5) summed to nonzero values that after the cross multiplication by Δt (in the Euler method), the finite digit addition to get the new θ_g resulted in a zero change. Thus, double precision on a 32-bit processor was required.

2.4. Model Evaluation for the Stable Boundary Layer

[38] Since this is largely a new model (although partly based on the structure of the single column model in *McNider and Pielke* [1981] and *Mackaro et al.* [2011]), we will provide an evaluation of the model and its components as we proceed through sensitivity experiments. In many instances, evaluation of boundary layer models involve running case studies from field program intensive periods [*André et al.*, 1978; *McNider and Pielke*, 1981; *Poulos et al.*, 2002;

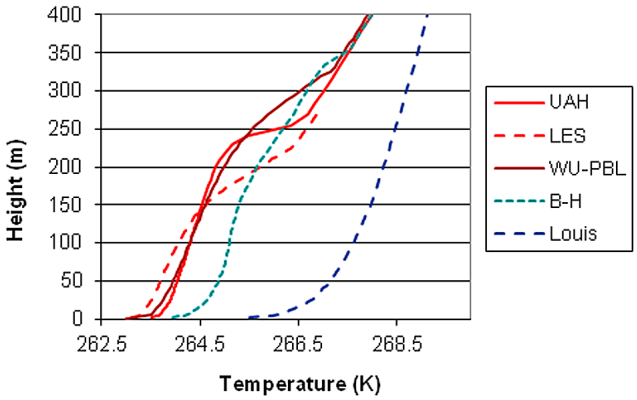

Figure 4. A posteriori comparison of the present model (UAH) against the GABLS1 single column model intercomparison [see *Cuxart et al.*, 2006]. LES came from the LES ensemble reported by *Cuxart et al.* [2006], WU-PBL is the Wageningen model [see *Steeneveld et al.*, 2006]. The B-H and Louis curves are runs with the UAH model using the Beljaars-Holtslag stability function and the Louis stability function.

Steeneveld et al., 2006]. However, as noted by *Byrkjedal et al.* [2008], tuning of models for particular in situ data can result in loss of generality of the parameterizations. With the present model, we are also limited in not being able to simulate the full diurnal cycle. Due to these issues, we will rely on the model evaluation structure carried out under the GEWEX GABLS1 model intercomparison protocols [*Holtslag*, 2006] and compare model behavior to other existing models that have been evaluated under the GABLS1 protocol [*Cuxart et al.*, 2006] and to models that have had extensive evaluation against several field data sets [*Steeneveld et al.*, 2006].

[39] The GABLS1 model intercomparison case is based on the simulations of an Arctic SBL by *Kosović and Curry* [2000]. The boundary layer is driven by an imposed geostrophic wind which is constant with height, with a specified constant surface cooling rate, and attains a quasi-steady state with a depth of between 150 and 250 m. It has also been used for a Large Eddy Simulation (LES) intercomparison [*Beare et al.*, 2006] aiming to quantify the reliability of stable boundary layer LES. The same grid prescription was retained for the single-column model intercomparison although weather forecast or climate models were run at their operational configuration.

[40] For the non-operational models, a vertical domain of 400 m was used with a grid mesh of 6.25 m (64 vertical levels), and a time step of 10 s, to reduce the differences originating from the numerical discretization. Instead of using the GABLS1 grid, we use the grid discretization that will be employed later for the GHG sensitivity experiments. Following the GABLS1 single-column protocol, a constant geostrophic wind with height, of 8 m s^{-1} in the x direction, was prescribed, and the latitude was 73°N (f = 1.39 × 10^{-4} s^{-1}). Radiation was switched off and the duration of the run was nine hours. See *Cuxart et al.* [2006] for additional details on the initial state and boundary conditions.

[41] Figure 4 shows the profiles of potential temperature from the GABLS1 intercomparison. Note that the present comparison is a posteriori comparison since in the original intercomparison modelers could not see other model runs. The present model employed in this study is referred to as UAH (after University of Alabama in Huntsville). This UAH designation uses the quadratic stability function suggested by England and McNider described previously. The LES designation is an aggregate of the LES models discussed by *Beare et al.* [2006] as reported by *Cuxart et al.* [2006]. The so-called Wageningen University PBL (WU-PBL) model is a model originally developed by *Duynkerke* [1991] and has been used extensively in stable boundary layer studies carried out at Wageningen University [*Steeneveld et al.*, 2006; *Holtslag et al.*, 2007]. This is also the model that will be used for comparisons to radiative forcing sensitivity later in the paper.

[42] The present model appears to compare favorably to the LES simulations in the mean profile of the boundary layer and in defining the top of the stable layer. The UAH model also compares favorably to the WU-PBL model. The somewhat better agreement of the UAH model at the top of the boundary layer with the LES model compared to the WU-PBL model may in part be due to a higher vertical-grid resolution (∼2–3 m grid spacing) near the top of the boundary layer in the UAH model than in the WU-PBL model, which used the GABLS1 intercomparison grid (∼6.5 m grid spacing)). The WU-PBL model also supports mixing at the top of the boundary layer even in very stable conditions.

[43] The remaining curves labeled B-H and Louis are runs of the UAH model with the Beljaars- Holtslag stability function and the Louis stability function as configured in the present model and shown in the appendix. The B-H and Louis forms have more mixing for the finer grid structure in the UAH model leading to greater downward heat flux and warmer surface temperatures as compared to the WU-PBL model. As will be discussed below, using the long-tailed forms for the stability functions in the fine grid as presented is perhaps not consistent with the intended use of these forms but does illustrate that the solution in the SNBL can be strongly dependent on the assumptions about mixing at larger *Ri*. This will be explored later when the partitioning of energy is compared between the mixing forms.

[44] The Wageningen model has been evaluated against several field data sets for the stable boundary layer [*Steeneveld et al.*, 2006, 2008a, 2008b; *van der Velde et al.*, 2010]. It has been shown to perform better than most operational models and research models in the stable boundary layer using a higher resolution than employed in the GABLS-1 comparison above. *Steeneveld et al.* [2011] also performed sensitivity experiments of the stable boundary layer to CO_2 forcing using this model. As we examine the sensitivity of the stable boundary layer to radiative forcing, we will evaluate the UAH model against the WU-PBL model. We feel this comparative sensitivity to forcing of the two models is a strict evaluation of the model's physics.

3. Model Sensitivity to Added Radiative Forcing Compared to the Two-Layer Dynamical System Model

[45] As discussed in the introduction, the bifurcation analysis of the simple dynamical system two-layer model by

Table 2. Soil Characteristics Used by *Walters et al.* [2007] Representing Dry Sand and Used in the Dynamical Analysis (Section 3.0) of the Present Paper

Characteristic	Value
Soil Density (ρ_s)	1600
Soil Specific Heat Capacity (c_s)	800
Soil Diffusivity (k_s)	2.3E-7
Soil Conductivity (λ_s)	0.3

Walters et al. [2007] showed that in certain parameter spaces, the model showed strong sensitivity to small changes in downward radiation. We explore this sensitivity using the full column model using the same turbulent parameterization as in the simple dynamical system model. We configure the parameters in the column model the same as the dynamical system model. As in the dynamical system model, we ignore clear air radiative cooling and use the simple downward radiation model given in equation (6). Table 2 provides the model soil parameters which are the same ones used in *Walters et al.* [2007] and correspond to dry sand [see *Pielke*, 1984]. Following *Steeneveld et al.* [2011], we use an initial thermodynamic sounding somewhat idealized from the CASES-99 field program [*Poulos et al.*, 2002]. The sounding is meant to capture a generic late afternoon sounding with a deep nearly adiabatic mixed layer. Since we want to evaluate the response to varying wind speeds, we impose a specified geostrophic wind speed as the initial wind speed profile above the boundary layer. In the boundary layer, we impose an initial Ekman wind profile to simulate the effects of daytime surface stress in the boundary layer. Imposition of such a sub-geostrophic profile is important for providing relatively balanced initial conditions and in treating the development and strength of an inertial oscillation [*Blackadar*, 1957] in and above the developing boundary layer.

[46] *Steeneveld et al.* [2011], in their sensitivity experiments, found their radiative transfer model produced an additional 4.8 W m^{-2} at the ground surface for an increase of 40% in CO_2. Our perhaps more complete radiative transfer model [*Fu and Liou*, 1993] indicated an added 1.8 W m^{-2}. This value seems more in keeping with the added radiative forcing from IPCC reports for CO_2 alone. *Kiehl* [2007] reports 3.7 W m^{-2} for a doubling of CO_2 which appears consistent with the *Fu and Liou* [1993] model. However, for consistency with *Steeneveld et al.* [2011] and because a value of 4.8 W m^{-2} is near the total increase in downward radiation including water vapor feedbacks in some postulated climate scenarios, we will use this as the added longwave forcing for all of our sensitivity studies. Following *Steeneveld et al.* [2011] and PM05, this added longwave energy could result from greenhouse gases as the reason for the added energy. But, in fact, added downward radiation from aerosols may also be of this order or more. For example, *Jacobson* [1997], in a modeling study, found an added longwave down of ~13 W m^{-2} for a case in southern California. In an observational study over the Indian Ocean, *Lubin et al.* [2002] found an increase of downwelling radiation of 7.7 W m^{-2} [see also *Nair et al.*, 2011].Thus, the added increment of energy used in the present study may be indicative of an increase in downwelling radiation from either greenhouse gases or aerosols or perhaps jet contrails [*Travis et al.*, 2004] or clouds [*Dai et al.*, 1999]. We should state explicitly that the simulations reported in this paper are not climate simulations in that we do not account for the accumulation of heat through a period longer than the nighttime period. Rather, following PM05 and *Steeneveld et al.* [2011] the experiments depict the response of a given SNBL to additional downward longwave forcing.

3.1. Development of Pseudo-Bifurcation Diagrams for Near-Surface Air Temperature

[47] Figure 5 shows the bifurcation diagram produced by numerical continuation reported in *Walters et al.* [2007] as the dashed lines. Wind speed is used as the bifurcation parameter. Note that as wind speed increases, there is an abrupt transition from a cold stable attractor solution to a warm stable attractor solution. The cold solution is associated with light winds and the warmer solution with windier conditions. Near the transition point multiple solutions (two stable and one unstable) are supported at larger roughness giving a classic "S" shape to the bifurcation diagram *Seydel* [1988]. Also, in this region, the solutions are unstable and complex eigenvalues are found, although not purely complex so that damped oscillatory solutions are supported. As discussed in *McNider et al.* [1995] and *Shi et al.* [2005], in this parameter space, the time dependent solutions are sensitively dependent on initial conditions. Explicit time dependent solutions of the dynamical system [see *McNider et al.*, 1995; *Shi et al.*, 2005] show an abrupt change as the solutions jump between the stable attracting solutions. The wind speed at which the transition occurs is referred to as the transition wind speed. *Van de Wiel et al.* [2002a, 2002b] found similar behavior in a simple model of the SNBL.

[48] We now explore whether this complex dynamical behavior is retained in a more complete multiple layer model. As noted above, we have constructed the single column model to mimic the boundary layer mixing of the dynamical model but made it more complete and realistic by including both a real skin temperature in the surface energy budget and an aerodynamic temperature for calculating the fluxes. Thus, we feel it is a close analogue to research grade boundary layer models such as *Steeneveld et al.* [2006].

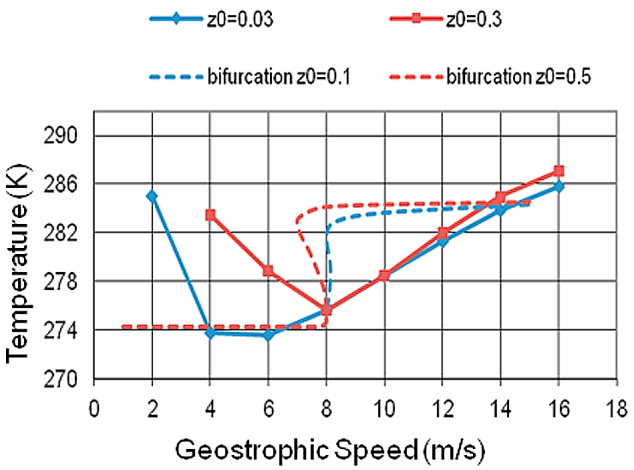

Figure 5. Dashed lines provide the bifurcation diagram reported in *Walters et al.* [2007]. Solid lines provide pseudo-bifurcation diagram for the UAH model with no clear air radiative cooling for two different roughness values.

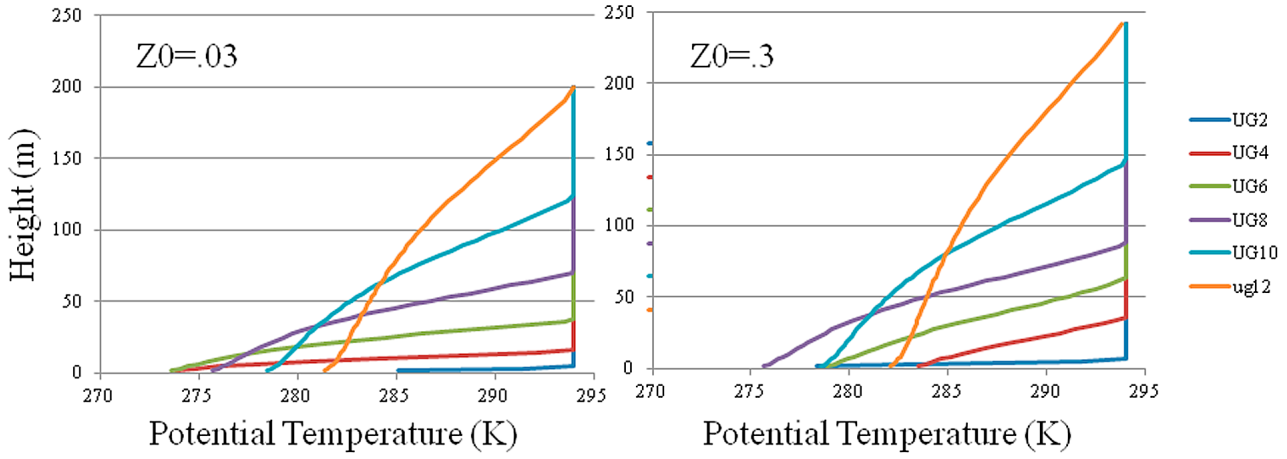

Figure 6. Vertical profiles of potential temperature for different imposed geostrophic velocities for the UAH model with no clear air radiative forcing.

[49] Figure 6 shows the temperature profiles for the idealized nocturnal boundary layer for different imposed geostrophic speeds for two different values of roughness. The boundary layer is deeper and less stable for the larger roughness. There is a fundamental change in the profile shape for light winds and strong winds above the surface. The light wind cases show an exponential type profile while the stronger wind cases show a parabolic like shape . From a simple differential equation view, this seems to indicate a transition of solutions from one functional form (perhaps dependent on the eigenvalues) as the SNBL moves from a strongly stable state to moderately stable state. This transition appears consistent with the dynamical system transition from the cold (calm) attractor to the warm (windy) attractor. This transition in shape has also been found in observations [e.g., *Van Ulden and Holtslag*, 1985; *Vogelezang and Holtslag*, 1996] and other nocturnal boundary layer models [*Mahrt*, 1999; *Edwards et al.*, 2006; *Weil*, 2011] as the boundary layer transitions from a very stable boundary layer to a weakly stable boundary layer.

[50] The behavior of the SNBL, especially near the surface under light winds, has been the subject of considerable theoretical debate [*Taylor*, 1971; *Derbyshire*, 1999; *Mahrt*, 1999] (and more recently, *Basu et al.* [2008]). *Derbyshire* [1999] provides a very nice discussion for the possibilities of the behavior of the near-surface profiles under extreme stability. Derbyshire pointed out that in the very stable boundary layer, the near-surface atmosphere can realize one of two states. The first state is one with strong ground surface cooling resulting in large near-surface vertical temperature gradients but turbulence is maintained by shear in the face of stability which drives a downward heat flux that keeps the surface turbulently connected. The second possible state is one in which the strong stability suppresses turbulence and leads to a decoupling of the atmosphere and the ground. We believe these two states are somewhat akin to the two attracting solutions found in the bifurcation diagram in Figure 5. In the two-layer dynamical system model, the two stable solutions correspond to a first state where the lowest model level in the atmosphere becomes coupled to the surface so that the air temperature collapses close to the temperature of the surface but decoupled from the outer atmosphere. This would correspond to Derbyshire's coupled state (near-surface temperature connected to ground surface). However, the second state in the dynamical two-layer model corresponds to a state where the first layer air temperature is coupled to the outer layer. The two-layer model, because of its reduced degrees of freedom, cannot resolve the case where the surface becomes decoupled from the ground surface.

[51] We now attempt to replicate the bifurcation diagram from *Walters et al.* [2007] (Figure 5) by examining the model temperature at the first model level (1.5 m ~approximately screen level) in the column as a function of imposed geostrophic winds. This pseudo-bifurcation diagram is depicted in Figure 5. In the present multilayer column model (for this particular soil state), it appears that the abrupt transition of states as seen in the bifurcation analysis (Figure 5) is somewhat muted compared to the two-layer dynamical system model and, in fact, it appears three regimes are supported. This shows a more complex behavior than the simple dynamical model. At the lighter wind speeds, there is little mixing, so at the extreme light winds, the boundary layer is weak, shallow, and cold air at adjacent to the surface cannot be lifted to the first level by turbulent mixing. This region corresponds to Derbyshire's decoupled state. As the imposed geostrophic speed increases to ~6−8 m s^{-1}, enhanced turbulent mixing lifts more cold air off the surface leading to colder solutions at the first model level. This is in the region of the more exponential shaped profile solution mentioned above and corresponds to Derbyshire's coupled state. However, as winds increase further, the surface temperature now begins to warm with increased wind speeds (this region is in the parabolic profile regime). This region corresponds to the weakly stable boundary layer [*Mahrt*, 1999; *Weil*, 2011] and corresponds to the two-layer solution of the coupling of the surface air temperature to the outer layer. Thus, while the more complete model is more complex in the bifurcation diagram replication, the simple dynamical system model was foretelling a transition between these latter two different states.

[52] In summary, the multilayer model supports three separate regimes - two in the very stable boundary layer and one in the weakly stable boundary layer. In the very stable boundary layer, both of Derbyshire's states exist. At very

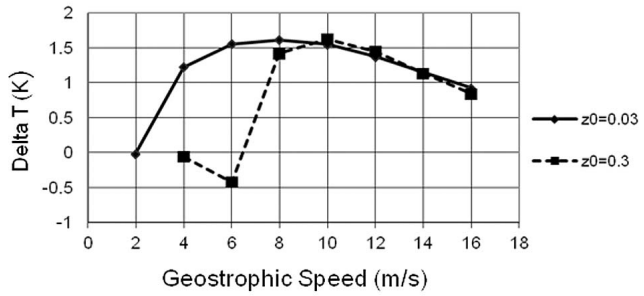

Figure 7. Differential change in temperature for the case of added longwave energy minus the base case versus wind speed for two different roughness values.

light winds the first model layer is decoupled from the ground surface. At slightly larger winds, the first layer becomes turbulently coupled to the ground surface. At even stronger winds (weakly stable boundary layer), the near surface becomes turbulently connected to the outer atmosphere. For a fixed wind speed the transition between these regimes in the multilayer model is a function of roughness. This is not the case in the two-layer dynamical system model and deserves additional analysis. As we will discuss later in the paper, models with greater levels of mixing do not capture the decoupling from the surface.

[53] While the multilayer column model provides some consistency with the two-layer bifurcation analysis and the warmer solutions at lighter winds are physically interpretable, the shape of the pseudo-bifurcation diagram is perhaps inconsistent with normal views and modeling of the SNBL. While SNBLs are complex, we feel most operational models would show a monotonic increase in shelter level temperature as wind speed increases. The somewhat odd sense of the present model's pseudo bifurcation diagram is due to the minimum level of mixing in the model and will be explored later after clear air radiative cooling is added in section 5.

3.2. Response of the SNBL to Added Downward Radiative Flux

[54] *Walters et al.* [2007] explored the dynamics of the simple system with added greenhouse gas forcing as a bifurcation parameter near the transition wind speed from the wind speed bifurcation diagram. In *Walters et al.*, 2007 the added energy bifurcation diagram shows an abrupt transition in the region of reasonable variations in greenhouse gas forcing and multiple solutions are supported. The abrupt transition means that even slight changes in greenhouse gas forcing can shift the solution to a warmer (and windier state). We should note that magnitude of the transition in the simple dynamical system model is dependent on the layer depth chosen in the two-layer model and in fact layer depth enters the dynamical system as a parameter [*Shi*, 1997].

[55] We now examine the response of the multilayer column model to added forcing by greenhouse gas forcing. We impose an added 4.8 W m^{-2} to the downwelling radiation from the atmosphere as discussed above and examine the differences in boundary layer behavior. Figure 7 shows the differences in first level (1.5 m) model temperature due to the added forcing as a function of wind speed. It can be seen that the magnitude of differential warming corresponds closely to the transition in states discussed above. For lighter winds, the turbulence is weak and the added heat cannot be efficiently lifted off the surface, so there is little change in temperature. For stronger winds, turbulence efficiently removes the added heat and deposits it in the atmosphere. To illustrate this concept, we calculate budgets to determine where the added heat ends up in the model system.

4. Model Energy Budgets

[56] The longwave energy added into the model system can be partitioned or deposited into several reservoirs. The added energy can go to heating the atmosphere or go to heating the slab (top ground layer). Also, there are losses of energy from the system. Energy radiated from the surface is lost to space and energy from the slab can be lost to the substrate (deeper ground layer). We calculate the energy budgets from the model for the system as a whole. The surface turbulent heat flux from the model is integrated over time to provide the turbulent heat gain or loss to the atmosphere (through the surface flux divergence). In the base state model, this is checked by also calculating the change in column energy by converting the temperature profile to a heat content profile (i.e., dry static energy) and then integrating the profile:

$$E_A = \int_0^{top} \rho c_p \theta dz$$

[57] Thus, the change in energy content for the atmosphere over the time length of integration (τ) is:

$$\Delta E_A = \int_0^{top} \rho c_p [\theta(\tau) - \theta(0)] dz$$

[58] Because the original simple two-layer model and the parallel column model did not carry along either an equation of state or pressure, a constant surface density was used for calculating surface heat flux (H_o). This is not a significant assumption for the shallow SNBL here. For consistency and since we are interested in the shallow SNBL, the energy integral assumes a constant density and the integral was limited to the lowest 1.5 km of the model. In the model without radiation, the only energy source for the atmosphere is the surface sensible heat flux so that the net input of energy over time (T) is:

$$\int_0^{\tau} H_o dt$$

where τ is the time of integration. These two independent measures of gain or loss for the atmosphere must balance:

$$Imbalance_A = \int_0^{top} \rho c_p [\theta(\tau) - \theta(0)] dz - \int_0^{\tau} H_o \ dt.$$

[59] Similar, calculations were made to determine the change in energy of the ground slab:

$$\Delta E_s = \rho_s \ c_s \ \Delta h \left[T_g(\tau) - T_g(0) \right]$$

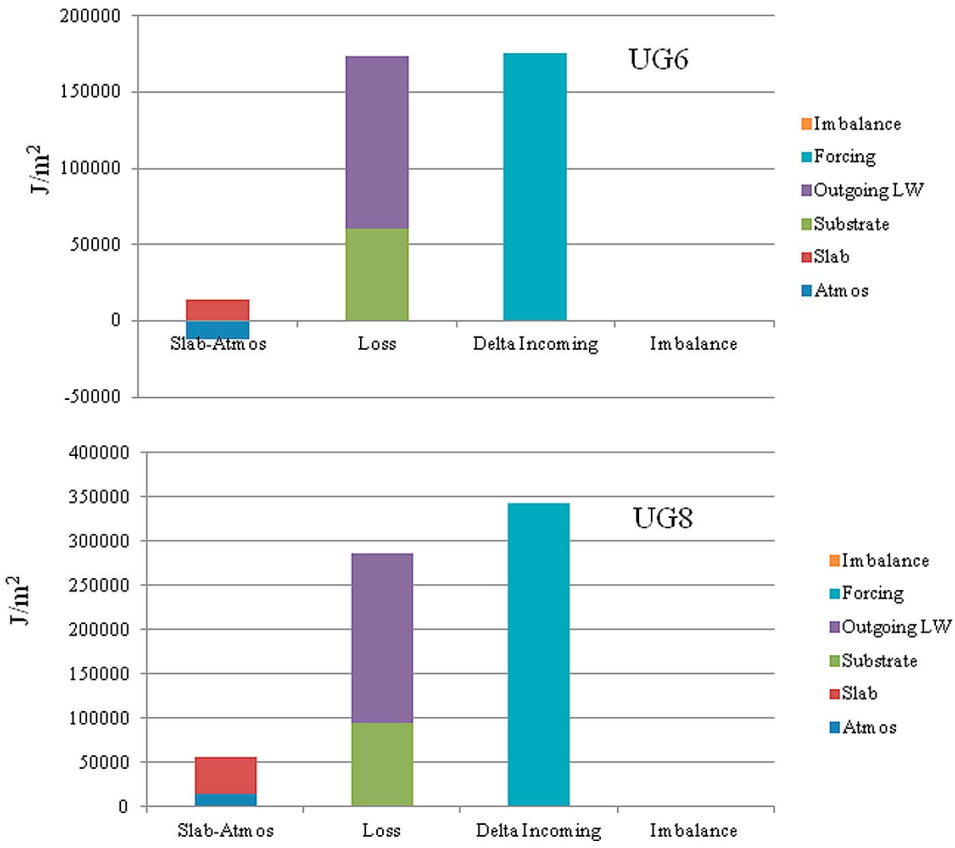

Figure 8. Model budget showing disposition of the added longwave energy (4.8 W m^{-2}) after 12 h of simulation for the UAH model for the case of no clear air radiative forcing. Note positive values indicate heat added and negative values a loss to each reservoir.

as well as the radiative losses from the slab:

$$E_o = \int_0^\tau \sigma \; T_R^4(t)dt$$

and conductive losses to the substrate:

$$E_m = \int_0^\tau \kappa_m \; \left(T_g(t) - T_m\right)dt.$$

[60] An equivalent balance for the slab is given by

$$Imbalance_s = \rho_s \, c_s \, \Delta h\left[T_g(\tau) - T_g(0)\right] - \int_0^\tau \sigma T_R^4 dt - \int_0^\tau \kappa_m\left(T_g(t) - T_m\right)dt$$

[61] In tests in the base case of the model (i.e., before adding the longwave increment), the total fractional balances (imbalance/totals) for the atmosphere and the slab were generally less than 0.005.

[62] Next, this budget framework was used to examine where the added longwave energy is partitioned or deposited within the system. However, the definition of added energy entails some ambiguity. While we add a fixed 4.8 W m^{-2} rate to the downwelling radiation from the atmosphere to the surface, the actual downwelling radiation can also be changed as the atmosphere responds to the added heat. In the simple model without a clear air radiative parameterization, the added downwelling radiation comes from equation (6) and is dependent on the first layer model temperature. Thus, as the first layer temperature heats up, the downward radiation increases (thus a positive feedback).

[63] Figure 8 shows the budget in total J/m^2 for the 0.3 m roughness case before and after the transition in states (UG6 and UG8). The atmospheric integral gain or loss is found by summing the total sensible heat flux over the simulation at the time step level. The radiative loss is found by summing the upwelling radiation from the surface at the time step level. The downwelling radiation and the loss to the substrate are similarly calculated.

[64] For the lighter wind speeds, the added energy evidently is not removed from the surface by turbulence to the atmosphere so the skin temperature increases and thus the added energy radiates from the surface as a loss to the system. The slab heats up, and there is a loss to the substrate and the budget balances. For the higher wind speeds, more of the added energy is transferred to the atmosphere as sensible heat. What is noticeable is that the downwelling energy significantly changes between the two cases due to the approximately 1.5 K warming of the first model layer.

[65] However, the question is how could the first level temperature increase by 1.5 K given the partitioning of

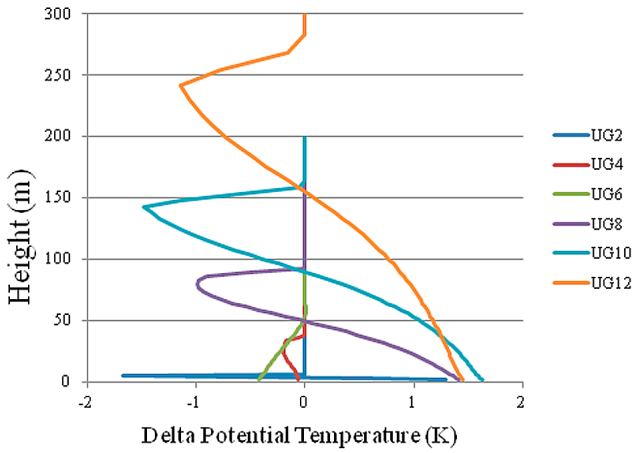

Figure 9. Difference in vertical potential temperature profile between added GHG energy and base case from UAH for the case with no clear air radiative cooling.

energy in which only a fraction of the energy added actually gets into the atmosphere. We can make a first order calculation of the change in boundary layer temperature by assuming the following simple model:

$$\Delta T = \frac{\Delta H}{\rho c_p h} \tag{14}$$

where is the change in boundary layer temperature, ΔH is the added heat, ρ is the air density, c_p is the air specific heat capacity and h is the boundary layer depth. *Esau* [2008] also noted that the response to forcing is inversely proportional to the boundary layer depth.

[66] For the total 12-h simulation, the direct incremental heat added to the system at a rate of 4.8 W m^{-2} is approximately 207,000 J/m^2. If all of this heat were added to the boundary layer with a boundary layer depth of approximately 100 m (from Figure 6), equation (14) yields a $\Delta T \sim 1.6$ K. However, the model budget indicates that only about 14,100 J/m^2 are introduced into the atmosphere as sensible heat which, for this model (with the absence of atmospheric radiative heating), is the only source of atmospheric heating. Using this heat input in the simple model yields a ~0.11 K. Then, the question arises: How can the column model surface air temperature (1.5 m level) increase by 1.5 K?

[67] The answer lies in a conjecture made by *Walters et al.* [2007] based on the simple dynamical system that the added greenhouse gas forcing destabilizes the boundary layer producing a slightly deeper nocturnal boundary layer but, more importantly, a slightly less stable profile. The growth of the boundary layer and less stable profile allows enhanced downward mixing of warmer air to the surface. This further increases the downwelling radiation. Thus, there is a substantial positive feedback to increase the near surface temperature. In this case, it is as though the 14100 J/m^2 has acted to be equivalent to ~200,000 J/m^2 in terms of the temperature response. However, as noted by *Walters et al.* [2007], this increase in temperature at the surface is due to a redistribution of heat in the atmosphere, not an accumulation of heat.

[68] To examine this redistribution in the full column model, Figure 9 shows the temperature profile difference between the base case and the added radiative forcing for different geostrophic wind speeds. One can see that at the UG6 case before the transition, there is very little change in the atmospheric profile between the two cases. However, in the UG8 difference profile it can be seen that there is a substantial change in the profile with cooling aloft and warming below. To help explain the difference, Figure 10 shows at higher resolution the actual temperature profiles for the UG8 case with and without the added radiative forcing and also shows the difference plot. The actual profiles show the boundary layer has been slightly destabilized by the added forcing, and the boundary layer has grown slightly. In some sense, the added forcing in destabilizing the boundary layer is acting in the same sense as a slightly increased wind speed. The slightly deeper and more turbulent boundary layer has redistributed heat in the profile with cooling aloft and

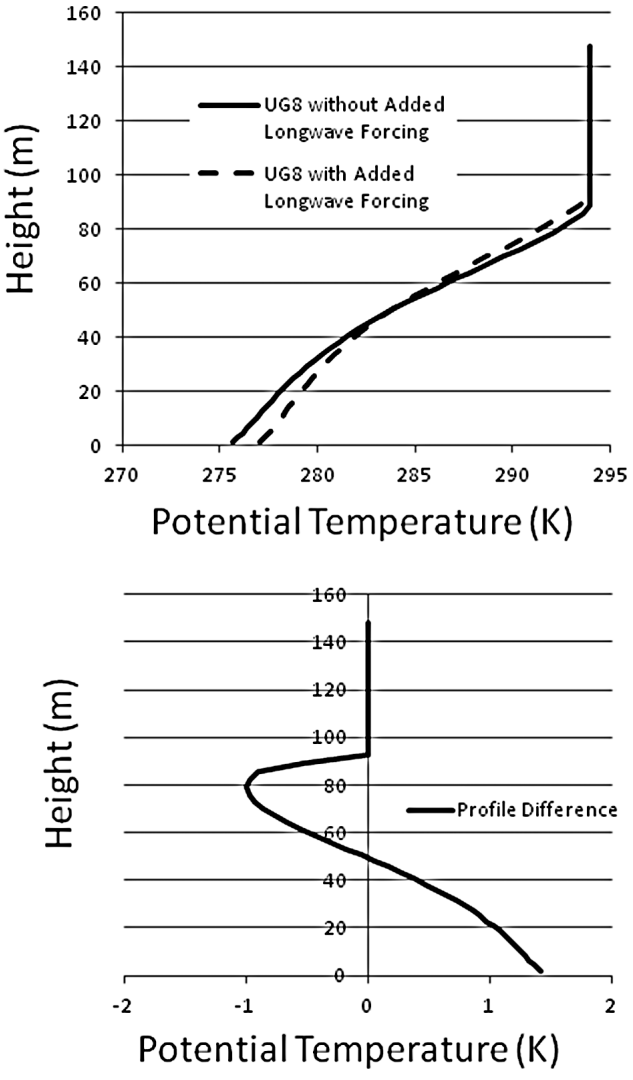

Figure 10. (top) Expanded view of the difference in potential temperature profile between the case of added GHG energy and base case for a geostrophic wind of 8 m s^{-1}. (bottom) Expanded view of profile difference.

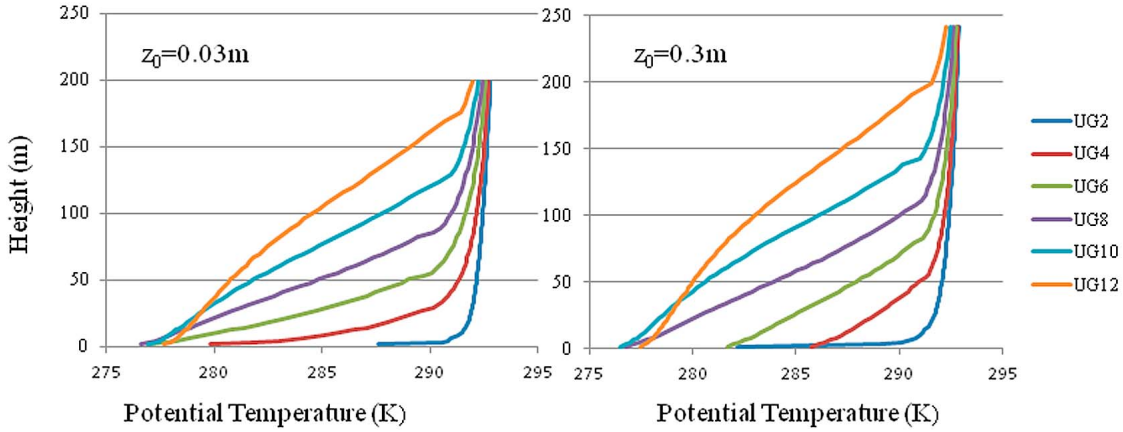

Figure 11. Vertical profiles of potential temperature for different imposed geostrophic velocities for the UAH model with clear air radiative forcing.

warming below. Again, this is analogous to a windier stable boundary layer mixing warm air to the surface. The amount of warming at the surface due to this redistribution of heat is reflected by the relative amount of area in the cooled and warmed areas. Thus, it can be seen that a large amount of the warming at the surface is due to this redistribution of heat, not to the added heat from the added radiative supplement.

[69] This integrated change in heat content was computed in the model. In carrying out this integration of the difference profile, we find that the net heating in the profile is 14400 J/m^2 or within the rounding and numerical error equivalent to the 14078 J/m^2 found by summing the sensible heat flux in the budget given in equation (6). Because mixing is a conservative process, by integrating the negative (cooled area) in the upper levels, we can also determine the amount of heating seen in the lower part of the profile that is due to this redistribution. In carrying out this integration, we find that ~30600 J/m^2 of the warming in the lower part of the profile is due to this redistribution of heat. Thus, we can see that the redistribution of heat accounts for well over twice the heating of the lower profile compared to the added heat from the radiative supplement. In the simple downward radiative model, the added downwelling energy to the surface is also driven by this warming leading to another positive feedback.

5. Model Response With Clear Air Radiation

[70] The original two-layer bifurcation analysis model and the full multilayer column model above neglect clear air radiative contributions as did the *Derbyshire* [1999] model. Clear air radiative contributions have been indicated to be a significant component in the development of the *nocturnal boundary layer* [*André et al.*, 1978; *McNider and Pielke*, 1981; *Garratt and Brost*, 1981; *Steeneveld et al.*, 2011]. We now examine the response of the stable boundary layer to external forcing with the inclusion of a full radiative scheme that allows both cooling through radiative flux divergence in the atmosphere as well as improved specification of downwelling longwave flux to the surface. The scheme incorporated is the *Fu and Liou* [1993] scheme, which is a Delta four-stream radiative transfer code.

[71] We add the radiative forcing for the same model case as described above. Figure 11 shows the vertical profiles of temperature for different wind speeds and for roughness lengths of 0.03 m and 0.3 m. It shows that radiation largely serves to smooth the profiles. The large and abrupt curvature at the top of the SNBL creates radiative flux divergence which smoothes the inflections. There is also now clear free air cooling of the profile above the turbulent boundary layer so that the effective inversion height is increased (compare to Figure 6). This is consistent with other studies showing the impact of clear air radiative contributions [*Garratt and Brost*, 1981; *McNider and Pielke*, 1981; *Steeneveld et al.*, 2006].

[72] We next examine the pseudo-bifurcation diagrams for the case with radiation. Figure 12 shows the dependence on temperature with wind speed for the roughness length of 0.3 m for the England-McNider (E-M) stability form as well as the Beljaars and Holtslag and Louis stability functions, which will be discussed later in the paper. The shape of the bifurcation diagram for the E-M form is similar to that with no clear air radiation included except, as with the vertical profiles, the curves are smoother, and there is not as much of an abrupt change at the transition. The case with radiation also has lower temperatures at higher wind speeds (compare with Figure 6). This is in part due to slightly reduced downward longwave radiation at the surface using the full radiative code.

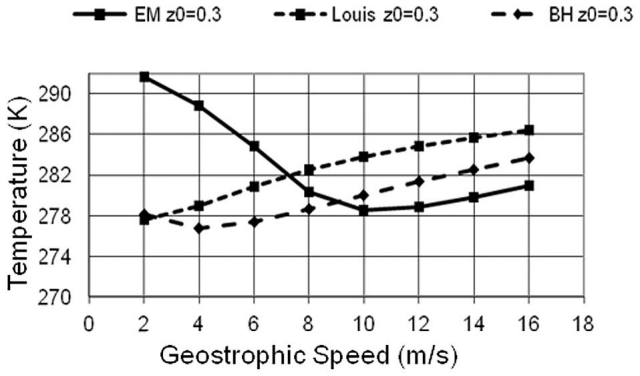

Figure 12. Pseudo-bifurcation diagram for the UAH model with clear air radiative cooling at using (EM) the England-McNider stability function, (BH) the Beljaars-Holtslag form and the Louis form.

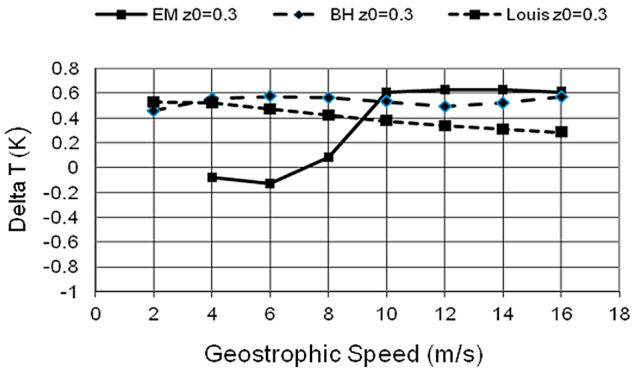

Figure 13. Differential heating for the case with clear air radiational forcing added radiative energy minus base case versus wind speed for different stability functions.

[73] As mentioned above, while the shapes of the E-M pseudo-bifurcation diagrams are physically interpretable, the perhaps more expected response is that shelter level temperatures would increase with increasing wind speed. We must remember that the present model was constructed to keep non-explicit (i.e., computationally caused) mixing to a minimum. Additionally, the E-M stability function supports minimum mixing compared to stability functions used in many operational models [*Viterbo et al.*, 1999; *Cuxart et al.*, 2006]. We must further caution that operational models operating at coarse resolution and for non-idealized settings may explicitly and implicitly incorporate other forms of mixing such as topographic drag [*Steeneveld et al.*, 2008b] and wave drag [*Chimonas and Nappo*, 1989]. Also, as noted above, *Delage* [1997] and *Mahrt* [1987] argued that grid averaged *Ri* are larger than point measurements. The present model while consistent with theoretical boundary layer over flat terrain may not fully reflect the complexities of the real world. To test the impact of increased mixing, we now run the model for the longer-tailed stability functions (the Beljaars and Holtslag and Louis forms).

[74] Figure 12 shows the pseudo-bifurcation diagram for the Louis and Beljaars-Holtslag form. As shown, with the additional mixing, the bifurcation diagrams show the perhaps expected behavior of temperature increasing with imposed wind speed. There is a slight tendency for the Beljaars-Holtslag form, which has less mixing than the Louis form, to also show warmer temperature at the lowest wind speed like the England-McNider form.

[75] As noted by *Delage* [1997] and *Derbyshire* [1999], even though the short-tailed stability functions appear to approximate best the classic surface layer profiles, many operational NWP settings have added mixing such as from the Louis and Beljaars-Holtslag form to reduce a cold bias in 2 m temperatures [*Viterbo et al.*, 1999]. However, in the present model with minimum non-turbulent mixing and the short-tailed stability function, the first level temperatures remain relatively warm at low wind speeds. In operational models and research models, minimum diffusion coefficients are often used ($K = 0\ m^2\ s^{-1}$ is actually an ill-posed problem). Also, minimum flux values or minimum u_* values are sometimes set in part to avoid division by zero in similarity expressions. Unless these are set to be sufficiently small, they can cause the first level to be turbulently connected to the surface. This results in the first model layer becoming too cold. Then, added mixing such as from a Louis or B-H form is needed to mix heat downward to reduce cooling at the first layer.

[76] We next carry out the added longwave energy experiments using the model with the clear air radiation included. Figure 13 (solid line) shows the differential heating due to added radiative energy as a function of wind speed for the model for the E-M stability function with clear-air radiative contributions included. The general characteristics of the curves are similar to the cases without radiation (Figure 7). There is a tendency for the heating to be less an inverse function of wind speed (i.e., flatter) at higher wind speeds. In tests where clear air radiation was used but downwelling radiation was calculated from the simple expression dependent on first level temperature used in *Walters et al.* [2007], we found that the change in behavior at higher wind speeds was due to the differences in downwelling radiation to the surface with the full radiation code and not to clear-air radiative contributions

[77] Figure 13 (dashed lines) show the response of the first level temperature when longer-tailed stability functions (Beljaars-Holtslag (B-H) and Louis) are used. The response of the air temperature in the longer-tailed forms does not depend as strongly on wind speed as does E-M. This is due to the increased level of mixing in the long-tailed forms more effectively lifting the added heat off the surface. In the E-M form, the connectivity to the surface is limited because of small turbulence levels, so the energy does not enter the atmosphere.

[78] Figure 14 shows the energy budgets for the model with full radiation included for a roughness of 0.3 m and the E-M, B-H, and Louis stability functions. One can see that the forms with more mixing are more effective in getting the added radiative energy off the surface and into the atmosphere. It also shows that the response of the atmosphere is less for the cases with more mixing. This is evidently due to the larger boundary layer heights in the models with more mixing. Even though these models are mixing the added energy off the surface more effectively, the energy is being distributed over a greater depth (see equation (14)).

[79] The most important difference is the much larger amount of energy added to the atmosphere compared to the model with less mixing (the E-M form). In the E-M form and its limited mixing, the added energy stays at the surface and is then more effectively radiated out and lost to the system (some small amount is absorbed in the atmosphere but most escapes through the window region). In the budget for the Louis UG8 case, over 90,000 J/m^2 are added to the atmosphere compared to $\sim$14,000 J/m^2 for the England-McNider UG8 case. While most of the warming at the first model level in the England-McNider form is due to the redistribution of heat in the profile, the forms with more mixing are heating due to an accumulation of heat from the additional surface heat flux.

[80] To be fair, the B-H and Louis forms were probably not intended to be applied in this fine resolution model setting. In coarser grid models, these forms would likely produce less mixing than what is given. However, these experiments show that added mixing, whether from numerical schemes

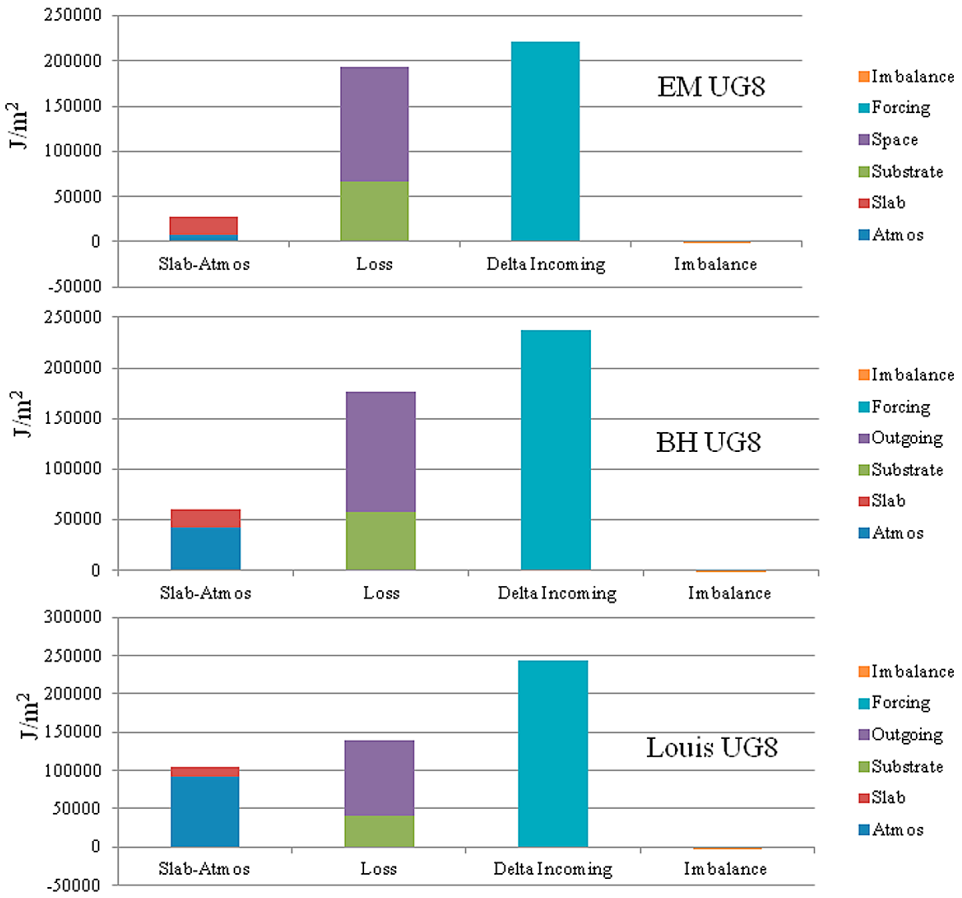

Figure 14. Model budget showing disposition of added longwave energy (4.8 W m^{-2}) after 12 h of simulation for the UAH model for the case of with clear air radiative forcing for the England-McNider (EM), Beljaars-Holtslag (BH) and Louis stability function. Note positive values indicate heat added and negative values a loss to each reservoir.

and coarse resolution or to make models perform better operationally, can dramatically alter the fundamental distribution and partitioning of energy in the atmosphere in the SNBL.

[81] The difference profiles for the clear-air radiative case were generically similar to those without clear air radiative contributions (Figure 9). The redistribution of heat due to the destabilization of the boundary layer by the radiative supplement was retained in the case with the full radiative scheme.

6. Warming of the Near-Surface Temperature as a Function of Wind Speed

[82] As mentioned in the introduction, there has been some controversy in the literature concerning the dependence of warming in the nighttime on wind speed. *Parker* [2004] and, in more detail, *Parker* [2006] indicated, since he found no dependence in nighttime warming in observational data between light wind nights and strong wind nights, that the warming was not due to urban heat island effects and thus must be a part of the greenhouse gas warming signal. *Pielke and Matsui* [2005] (PM05), using a simple analytical model of the structure and character of the stable boundary developed by *Stull* [1983], found that added forcing from greenhouse gases yielded a near-surface temperature response that, like the urban heat island system, was also inversely dependent on wind speed.

[83] PM05 performed several experiments with the flux divergence (radiative and turbulent heat flux) varying from -50 W m^{-2} to -10 W m^{-2} showing the profile forms and lapse rates in the stable boundary layer for different wind speeds after 12 h. They then performed a greenhouse gas forcing experiment by showing the difference in temperatures between the -50 W m^{-2} and -49 W m^{-2} cases so that the greenhouse gas perturbation corresponded to a $+1.0$ W m^{-2} increase in energy in the boundary layer.

[84] *Steeneveld et al.* [2011] revisited the PM05 results using a more complete boundary layer model. This model included a fully interactive land surface model coupled to a first order closure atmospheric boundary layer model. The model was set up to partially mimic 23–24 October 1999 UTC during the CASES-99 campaign. The initial profile was inspired from the radiosonde of 23 October 1900 UTC, with an approximately constant potential temperature (284 K) from the surface to z = 800 m, and an inversion aloft. The specific humidity was taken constant (1.0 g kg^{-1}) in the whole model domain for the default experiment. The initial wind speed was constant with height and equal to the V_g, but matching a logarithmic profile close

Table 3. Soil Characteristics From *Steeneveld et al.* [2011] and Employed in the UAH Model in the Wind Speed Analysis in Section 4

Characteristic	Value
Soil Density (ρ_s)	1850 kg m^{-3}
Soil Specific heat capacity (c_s)	2150 J K^{-1} kg^{-1}
Soil Diffusivity (k_s)	1.55E-6 $m^2 s^{-1}$
Soil Conductivity (λ_s)	0.61 J s^{-1} m^{-1} K^{-1}

to the surface. This is similar to the idealized CASES-99 profile employed by the UAH model in the previous section, except the UAH case used a late afternoon sounding 23 October 0000 UTC and the actual specific humidity from the CASES sounding. *Steeneveld et al.* [2011] used the drier constant (1.0 g kg^{-1}) value because clouds formed in the S11 model with the original moisture which complicated the analysis. The UAH model does not have cloud processes, so this was not an issue.

[85] The UAH model in this section is configured to the soil parameters used in the *Steeneveld et al.* [2011] study rather than the dry sand soil in the above analyses (see Table 3). However, the treatment of the land surface in the *Steeneveld et al.* [2011] model is quite different from the UAH model. As we discussed previously, the UAH model employs a simple single slab model, but with a skin temperature coupled with the *Zilitinkevich* [1970] adjustment to compute fluxes. The *Steeneveld et al.* [2011] model uses a multilayer soil model but employs a vegetative mulch layer above the soil with a small heat capacity to give a large dynamic range in the surface temperature. *Steeneveld et al.* [2011] also uses the adjustment in roughness length for heat ($z_{0H} = z_{0M}/10$) in the flux calculations rather than an explicit adjustment. Also, the radiation codes are entirely different with the *Steeneveld et al.* [2011] model using a form of the *Garratt and Brost* [1981] radiative scheme, while UAH used the *Fu and Liou* [1993] code. While the radiative codes are different, as for the experiments in section 3, the UAH model employed the delta longwave supplement from *Steeneveld et al.* [2011] of 4.8 W m^{-2}.

[86] Figure 15 shows the *Steeneveld et al.* [2011] results compared to the UAH model. The *Steeneveld et al.* [2011] model effectively uses the Duynkerke stability function shown in Figure 3. However, it does not directly use the stability function formulation used in the UAH model; rather, it employs the more traditional iterative implementation [*Duynkerke*, 1991]. The UAH model was also run using the Ri dependent Duynkerke stability function.

[87] Given the differences in structure and inputs the two models agree well in terms of the dependence on wind speed. The UAH model appears to have less mixing than the *Steeneveld et al.* [2011] model and accentuates the muted response at smaller wind speeds where, as discussed above, the limited mixing inhibits the lifting of the added energy from the surface. But more importantly, the UAH model mostly confirms the conclusions of *Steeneveld et al.* [2011] that the response to added radiative forcing is largely independent of wind speed, particularly at speeds greater than ~4 m per second, and if there is any dependence, it is of the opposite sign proposed by PM05 at light wind speeds.

[88] *Steeneveld et al.* [2011], in questioning the PM05 temperature wind speed dependence, noted that the assumption of an added flux (+1.0 W m^{-2}) representing greenhouse gas forcing, while perhaps a first attempt at boundary layer sensitivity, was not realistic. Invoking observations and model results, *Steeneveld et al.* [2011] showed that the added flux must be dependent on wind speed. We here examine the role of fluxes as well as the nonlinear dynamics of the SNBL in the near surface temperature response.

[89] Figure 16 (top) shows the surface turbulent sensible heat flux from both the Steeneveld model and the UAH model (for both the Duynkerke stability function and the England-McNider form) for the base case without added radiative forcing. The fluxes agree relatively well with the UAH model showing slightly less flux at higher wind speeds. Figure 16 (bottom) shows the difference in sensible heat flux due to the added longwave energy. Given all the differences in the construction of the surface structures between the two models, the agreement in fluxes is heartening in that despite the highly nonlinear characteristics of the SNBL, a critical subcomponent of the models agree. We note that the peak in fluxes from the Steeneveld model near 14 m/s is likely a model aberration but since it was in the original model output and not from post-processing it is included in the plot.

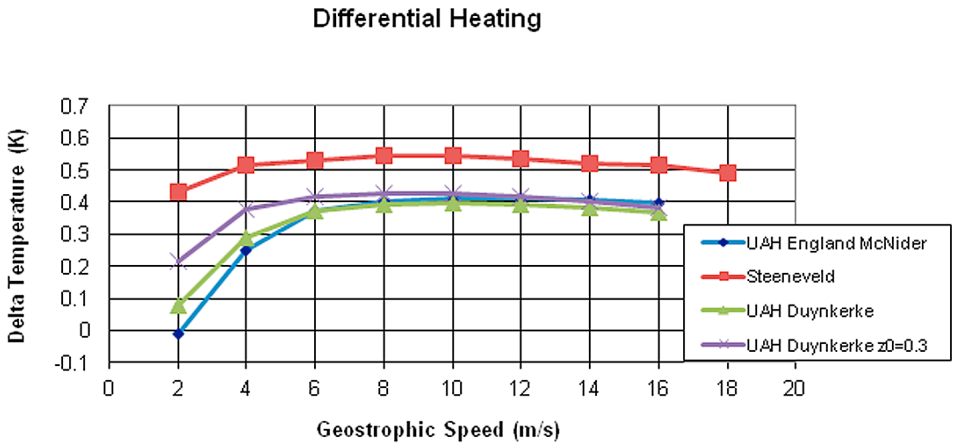

Figure 15. Differential heating – added longwave energy minus the base case versus wind speed for the *Steeneveld et al.* [2011] soils case with clear air radiational forcing.

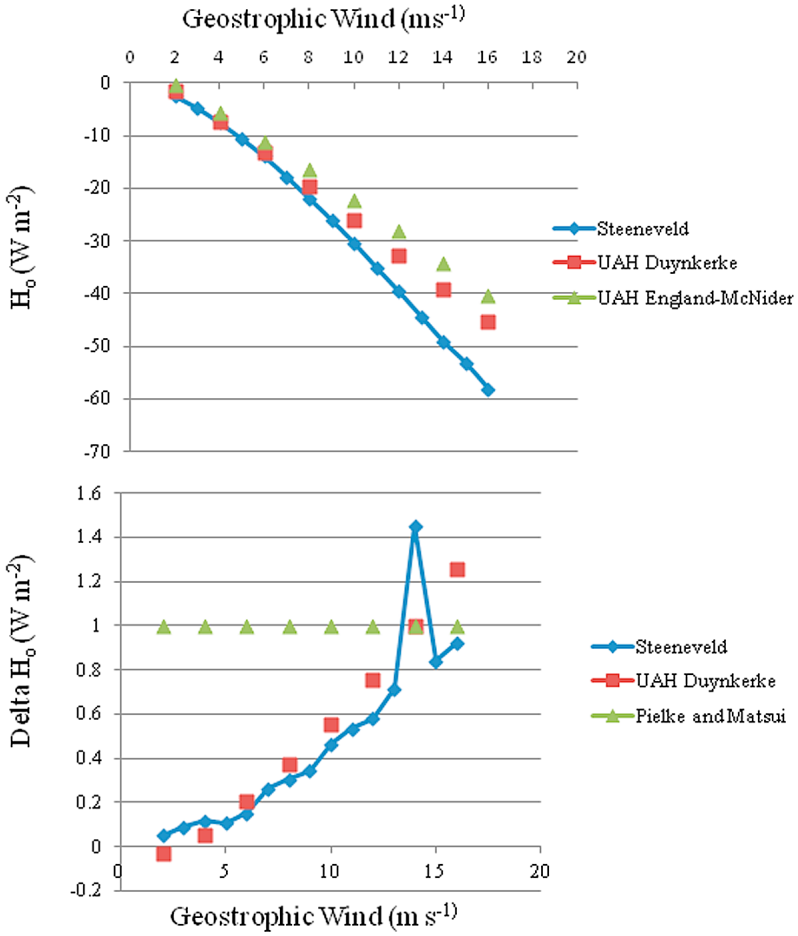

Figure 16. (top) Surface sensible heat flux comparison for the base case between UAH and the Steeneveld model. (bottom) Difference in heat flux (added longwave case minus the base case).

[90] *Steeneveld et al.* [2011] in their criticism of the PM05 results concluded that the neglect of land surface coupling and the resulting dependence of surface fluxes on wind speed were at the heart of the differences in model response. Figure 16 (bottom) also includes the simple constant flux used by PM05. However, the model results in the first part of this paper suggest that changes in the turbulent characteristics and temperature profiles in the SNBL itself may also play a role.

[91] The fluxes from the *Steeneveld et al.* [2011] model can be used directly in the Stull model employed by PM05. Figure 17 shows the surface 2 m air temperature from the Stull model using both the original constant flux used by PM05 and the fluxes from the Steeneveld model (in Figure 16). The Stull model response, even with the speed dependent fluxes, is quite different than the *Steeneveld et al.* [2011] model or the UAH model. The difference is that the Stull model does not include the role of nonlinear dynamics that added forcing plays in changing the shape of the profile and resulting redistribution of heat in the profile. The Stull model was developed as a first order model for the vertical behavior of temperature in the SNBL. Its exponential shape is more representative of the strongly stable boundary layer than the weakly stable boundary layer and was perhaps never

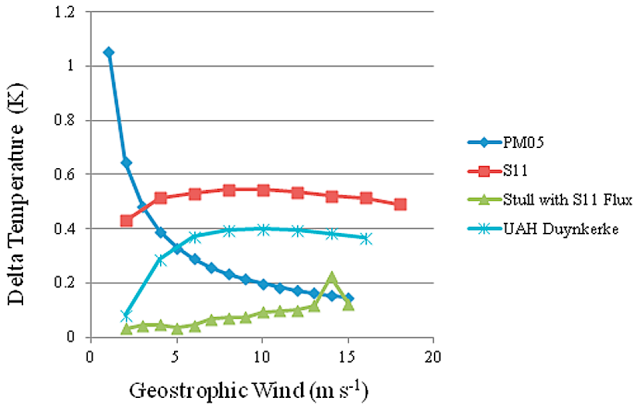

Figure 17. Difference in shelter level temperature due to added greenhouse energy. PM05 employs the Stull model and original increment of +1 W m^{-2} as used in *Pielke and Matsui* [2005]. S11 is from *Steeneveld et al.* [2011] and employs a GHG of 4.8 W m^{-2}. Stull with S11 flux uses the differential flux from Steeneveld *et al.* seen in Figure 16.

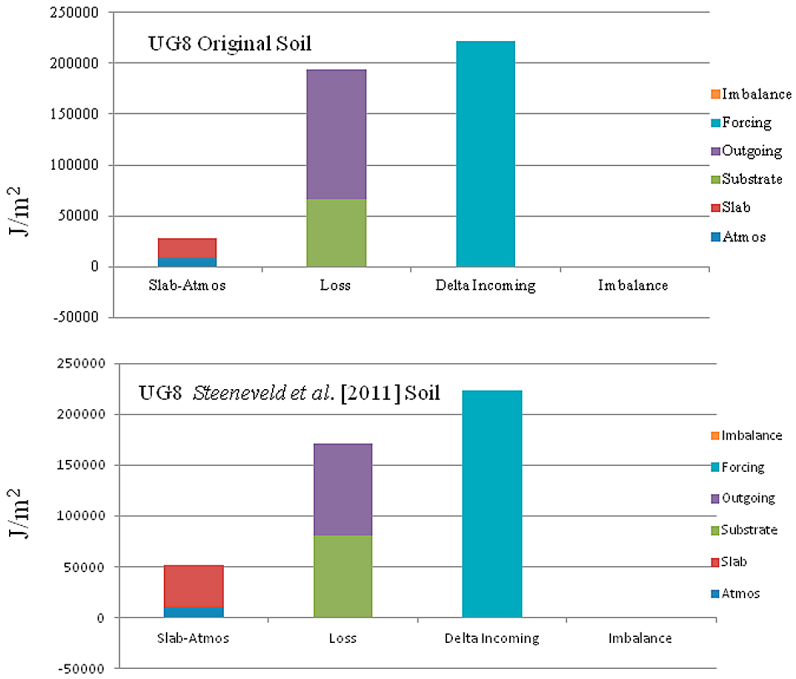

Figure 18. Model budgets showing disposition of added longwave energy (4.8 W m^{-2}) after 12 h of simulation for the UAH model for the case of with clear air radiative forcing comparing *Steeneveld et al.* [2011] soil which has larger soil conductivity than the original soil in Figures 8 and 14. Note positive values indicate heat added and negative values a loss to each reservoir.

intended to be applied across the range of wind speeds employed by PM05.

[92] *Steeneveld et al.* [2011] also postulated that the degree of land surface coupling might also determine the atmospheric response to added forcing. The *Steeneveld et al.* [2011] model employs a connection between their vegetative mulch layer and the soil using their ground heat flux - $G = \Lambda\ (T_{veg}–T_{s,0})$, where $T_{s,0}$ is the soil temperature of the topsoil and Λ is the land surface coupling coefficient. The UAH model, which employs a skin temperature, has a similar term, $G = \rho_s c_s k_s(\theta_s - T_G)\Delta h_{eff}^{-1}$, which connects the skin temperature to the slab. In the present paper the UAH equivalent land surface coupling coefficient for the original soil case (see section 3.0) is $\Lambda = 6$ Wm^{-2} K^{-1} and for the *Steeneveld et al.* [2011] soils in this section $\Lambda = 12$ W m^{-2} K^{-1}. This is somewhat larger than *Steeneveld et al.* [2011] who used $\Lambda = 5$ W m^{-2} K^{-1}. However, the *Steeneveld et al.* [2011] ground heat flux is connecting the vegetative mulch layer to the soil, whereas, in the UAH model, it connects the skin temperature to the soil. The skin temperature likely has a larger dynamic range than the vegetative mulch layer in *Steeneveld et al.* [2011]. As noted by [*McNider et al.*, 2005] the heat capacity or thermal inertia of actual grids with mixtures of soil, trees, mulch are really model heuristics not as simple as single soil or mulch configurations considered here.

[93] The only difference between the UAH model results in the first part of this paper (Figure 7) and the results compared to the *Steeneveld et al.* [2011] model (Figure 15) are in the soil parameters. While the soil density and heat capacity are different, the biggest effective difference is in soil conductivity which is twice that used in the experiments above (compare Tables 2 and 3).

[94] Using the budget tool, we can now examine how soil characteristics can change the partitioning of energy. Figure 18 shows the budgets for the two different soils (both have roughness $z_0 = 0.03$). One can see that the greater soil conductivity provides a larger part of the added longwave energy to the slab. The radiative loss is less. With the larger conductivity, the skin temperature does not cool as much, so the surface layer is less stable than the original soil. The model thus moves more quickly to a coupled regime. Therefore the model basically transitions faster. There is a caveat to the results in the UAH model in that the slab depth is fixed for these experiments. Thus, the effective land surface coupling coefficient is tied to this depth. Additional work should be carried out related to this model when sensitivity to land use change is addressed in a follow-on paper.

[95] This experiment and those with different mixing parameterizations show that both the atmospheric response and the ultimate fate of added energy depend strongly on the land surface characteristics as suggested by *Steeneveld et al.* [2011]. The previous experiment indicates that the turbulent treatment can also impact the response (see Figure 14). Thus, these model results indicate that the disposition of added heat is dependent on land use and mixing parameterizations.

7. Summary

[96] Due to the observed trend in diurnal temperature range, with a significant part of the warming in the observational record over land occurring at night, it is important to

understand the response and sensitivity of the SNBL to added radiative forcing. The present paper has performed a careful analysis of the behavior of the SNBL when subjected to an added increment of longwave forcing. It extended the simple two-layer bifurcation analysis of *Walters et al.* [2007] to a relatively complete multilevel single column model with a state-of the-science radiative scheme. This new column model was based on a new non-iterative boundary layer scheme which allows easy testing for different stability functions.

[97] The results show that the shelter level temperature in the SNBL can be quite sensitive to added radiation. In fact, the temperature changes on the order of 0.3−0.6 K due to a radiative forcing of 4.8 W m^{-2} would account for 50% of the trend in the instrumental record for the 20th Century (Figure 1). It would also be nearly equivalent to the warming produced by most climate models of 0.5 to 0.7 K over the 20th Century [*Kiehl*, 2007]. However, these experiments are not climate experiments since heat is not allowed to accumulate over a long-term integration. Rather, they show that, with all other variables being the same, a SNBL subjected to a small increment of energy would cause the shelter temperature to warm significantly while cooling the top portion of the SNBL. The increase in temperature is largely a result of the redistribution of heat in the profile, not in the accumulation of heat. Thus, even if heat had not accumulated in the deep atmosphere in the last century but longwave radiative forcing had increased (from either greenhouse gases or downward longwave radiation from aerosols or even jet contrails), we might expect a significant trend in minimum temperatures at shelter height.

[98] Based on the simple bifurcation analysis, *Walters et al.* [2007] speculated that in certain parameter spaces the SNBL might be destabilized by the added radiative increment producing a redistribution of heat. This redistribution of heat would then increase the surface temperature well beyond what the direct added energy would provide. This positive feedback conjecture was supported in the full column model.

[99] The analysis also showed that the final disposition and partitioning of the added energy in these short time period runs were highly dependent on the amount of mixing incorporated in the boundary layer scheme. These analyses illustrate that, in climate and weather models, care must be taken to ensure that mixing processes reflect the physics of the boundary layer rather than having mixing processes tuned to replicate single level observations. While operational and some climate models are sometimes tuned by adding mixing (based on the arguments of heterogeneity and missing processes) to make operational performance better in the SNBL [*Delage*, 1997; *Derbyshire*, 1999; *Viterbo et al.*, 1999], the results here indicate that climate models cannot perhaps afford this luxury in that such actions may also alter the disposition of added heat in the atmosphere and the energy budget of the atmosphere.

[100] The analysis also examined the shelter level temperature response to radiative forcing as a function of wind speed that had previously been addressed by *Pielke and Matsui* [2005] and *Steeneveld et al.* [2011]. The results broadened the parameter space analyzed by *Steeneveld et al.* [2011] in both roughness and land surface coupling. The conclusions are in agreement with *Steeneveld et al.* [2011] that the shelter level temperature change is largely independent of wind speed and counter to that of *Pielke and Matsui* [2005]. In fact, it was encouraging that internal details such as fluxes of the single column model and *Steeneveld et al.* [2011] agreed, even though the model structures were different and independent. The analysis also showed that the analytical Stull model [*Stull*, 1983] used by *Pielke and Matsui* [2005] even with specification of correct fluxes suggested by *Steeneveld et al.* [2011] does not incorporate the nonlinear dynamics needed to address properly the SNBL behavior when subjected to added radiative forcing.

[101] The present analysis reinforces previous work showing that the SNBL is a very complex dynamical system [*ReVelle*, 1993; *McNider et al.*, 1995; *Van de Wiel et al.*, 2002a, 2002b; *Delage*, 1997; *Derbyshire*, 1999] that can be highly sensitive to parameters appearing in the land surface coupling and to imposed parameters such as radiation and wind speed. Given the relatively shallow nature of the SNBL and our current understanding of how to parameterize turbulence, high vertical grid resolution appears to be the key to capturing the fidelity of the SNBL [*Steeneveld et al.*, 2006; *Byrkjedal et al.*, 2008]. Accurately addressing the SBL may also be critical to correct a warm bias in surface air temperatures in climate models in the Arctic [*Byrkjedal et al.*, 2008] and to the response of the Arctic SBL to added downward radiation of aerosols [*Nair et al.*, 2011].

[102] As noted above results here are not climate simulations and it is not entirely clear how the single column model results extrapolate to actual climate trends over land. However, in the absence of other information it appears that processes described here may alter such trends. Without true climate simulations we cannot determine if such processes might have other impacts on the larger scale circulation.

8. Discussion and Recommendations

[103] Since modeling of the SNBL is important to understanding climate change both in observations and models, it is imperative that models are developed and tested to ensure that climate trends and model trends agree physically in terms of the disposition and distribution of heat. While the present paper addresses the response and sensitivity of radiative forcing, additional work is needed to understand the response and sensitivity of the SNBL to land use change [*Pielke et al.*, 2007].

[104] Finally, one must remember that for all the detail and analysis carried out here, the surface characterization in both the UAH model and *Steeneveld et al.* [2011] model may be poor reflections of the complexities of the real world which must be modeled with amalgams of roughness, vegetation, soils, and topography with high resolution horizontal spatial grids [*McNider et al.*, 2005]. However, as pointed out by *Derbyshire* [1999], the theoretical and model frameworks, though somewhat disjointed from the complexities of actual fluid flows and observations, are the only tools we can build upon.

[105] Until we can better understand the causes of the trends in minimum temperatures and improve the ability of models to replicate these trends, the climate community should be cautious on the use of minimum temperatures as part of a greenhouse gas global warming metric. Given the sensitivity and current uncertainty in modeling of the SNBL, the climate community might consider that, if surface

temperature trends are going to be used as a metric to diagnose global warming, that trends in maximum temperatures (which sample a much deeper part of the atmosphere) would be more representative. As noted at the beginning of this paper, climate models have not in general replicated the nighttime warming. Given the coarse resolution in global models and corresponding difficulties in resolving the sensitivity of the shallow nighttime boundary layer, such replication of the nighttime warming may be out of the reach of current models. Thus, it may be better for current climate models, when they test replication of past climates and to project future global warming, to only use maximum temperatures rather than the current metric of using the mean daily temperature, which contains the minimum temperature. Of course, changes in nighttime temperatures represent real changes and possible impacts to the climate system (e.g., melting ice), to society (agricultural productivity) and to ecosystems. Thus, ultimately we need to develop climate models that do have the resolution and sensitivity to capture changes in minimum temperatures.

[106] **Acknowledgments.** Roger Pielke Sr. acknowledges support from NSF grant 0831331. Whitney Guerin is recognized for her excellent support in manuscript preparation. Dallas Staley completed the final editing of the paper with her standard outstanding work. We also recognize an anonymous reviewer who did a detailed review and provided numerous suggestions to improve the manuscript.

References

Acevedo, O. C., and D. R. Fitzjarrald (2001), The early evening surface layer transition: Temporal and spatial variability, *J. Atmos. Sci.*, *58*, 2650–2667, doi:10.1175/1520-0469(2001)058<2650:TEESLT>2.0.CO;2.

André, J. C., G. D. Moor, P. Lacarrere, G. Therry, and R. D. Vachat (1978), Modeling the 24-hour evolution of the mean and turbulent structures of the planetary boundary layer, *J. Atmos. Sci.*, *35*, 1861–1883, doi:10.1175/1520-0469(1978)035<1861:MTHEOT>2.0.CO;2.

Basu, S., A. A. M. Holtslag, B. J. H. van de Wiel, A. F. Moene, and G.-J. Steeneveld (2008), An inconvenient "truth" about using sensible heat flux as a surface boundary condition in models under stably stratified regimes, *Acta Geophys.*, *56*, 88–99, doi:10.2478/s11600-007-0038-y.

Beare, R. J., et al. (2006), An intercomparison of large-eddy simulations of the stable boundary layer, *Boundary Layer Meteorol.*, *118*(2), 247–272, doi:10.1007/s10546-004-2820-6.

Beljaars, A. C. M., and A. A. M. Holtslag (1991), On flux parametrization over land surfaces for atmospheric models, *J. Appl. Meteorol.*, *30*, 327–341, doi:10.1175/1520-0450(1991)030<0327:FPOLSF>2.0.CO;2.

Blackadar, A. K. (1957), Boundary layer wind maxima and their significance for the growth of nocturnal inversions, *Bull. Am. Meteorol. Soc.*, *38*, 283–290.

Blackadar, A. K. (1979), High resolution models of the planetary boundary layer, *Adv. Environ. Sci. Eng.*, *1*, 50–85.

Brohan, P., J. J. Kennedy, I. Harris, S. F. B. Tett, and P. D. Jones (2006), Uncertainty estimates in regional and global observed temperatures changes: A new data set from 1850, *J. Geophys. Res.*, *111*, D12106, doi:10.1029/2005JD006548.

Businger, J. A., J. C. Wyngaard, Y. Izumi, and E. F. Bradley (1971), Flux-profile relationships in the atmospheric surface layer, *J. Atmos. Sci.*, *28*, 181–189, doi:10.1175/1520-0469(1971)028<0181:FPRITA>2.0.CO;2.

Byrkjedal, Ø., I. Esau, and N. G. Kvamstø (2008), Sensitivity of simulated wintertime Arctic atmosphere to vertical resolution in the ARPEGE/IFS model, *Clim. Dyn.*, *30*, 687–701, doi:10.1007/s00382-007-0316-z.

Cao, H. X., J. F. B. Mitchell, and R. Lavery (1992), Simulated diurnal range and variability of surface temperature in a global climate model for present and doubled CO_2 climates, *J. Clim.*, *5*, 920–943, doi:10.1175/1520-0442(1992)005<0920:SDRAVO>2.0.CO;2.

Chimonas, G., and C. J. Nappo (1989), Wave drag in the planetary boundary layer over complex terrain, *Boundary Layer Meteorol.*, *47*, 217–232, doi:10.1007/BF00122330.

Christy, J. R., W. B. Norris, K. Redmond, and K. P. Gallo (2006), Methodology and results of calculating central California surface temperature trends: Evidence of human-induced climate change?, *J. Clim.*, *19*, 548–563, doi:10.1175/JCLI3627.1.

Christy, J. R., W. B. Norris, and R. T. McNider (2009), Surface temperature variations in East Africa and possible causes, *J. Clim.*, *22*, 3342–3356, doi:10.1175/2008JCLI2726.1.

Cuxart, J., et al. (2006), Single-column model intercomparison for a stably stratified atmospheric boundary layer, *Boundary Layer Meteorol.*, *118*(2), 273–303, doi:10.1007/s10546-005-3780-1.

Dai, A., K. E. Trenberth, and T. R. Karl (1999), Effects of clouds, soil moisture, precipitation and water vapor on diurnal temperature range, *J. Clim.*, *12*, 2451–2473, doi:10.1175/1520-0442(1999)012<2451:EOCSMP>2.0.CO;2.

Deardorff, J. W. (1972), Theoretical expression for the countergradient vertical heat flux, *J. Geophys. Res.*, *77*, 5900–5904, doi:10.1029/JC077i030p05900.

Delage, Y. (1997), Parameterising sub-grid scale vertical transport in atmospheric models under statically stable conditions, *Boundary Layer Meteorol.*, *82*, 23–48, doi:10.1023/A:1000132524077.

Derbyshire, S. H. (1999), Boundary-layer decoupling over cold surfaces as physical boundary instability, *Boundary Layer Meteorol.*, *90*, 297–325, doi:10.1023/A:1001710014316.

Doedel, E. J., H. B. Keller, and J. P. Kernevéz (1991), Numerical analysis and control of bifurcation problems: (I) Bifurcation in finite dimensions, *Int. J. Bifurcat. Chaos*, *1*, 493–520, doi:10.1142/S0218127491000397.

Durre, I., and J. Wallace (2001), Factors influencing the cold season diurnal temperature range in the United States, *J. Clim.*, *14*, 3263–3278, doi:10.1175/1520-0442(2001)014<3263:FITCSD>2.0.CO;2.

Duynkerke, P. G. (1991), Radiation fog: A comparison of model simulation with detailed observations, *Mon. Weather Rev.*, *119*, 324–341, doi:10.1175/1520-0493(1991)119<0324:RFACOM>2.0.CO;2.

Easterling, D. R., et al. (1997), Maximum and minimum temperature trends for the globe, *Science*, *277*, 364–367, doi:10.1126/science.277.5324.364.

Edwards, J. M., R. J. Beare, and A. J. Lapworth (2006), Simulation of the observed evening transition and nocturnal boundary layers: Single column modelling, *Q. J. R. Meteorol. Soc.*, *132*, 61–80, doi:10.1256/qj.05.63.

Ek, M. B., K. E. Mitchell, Y. Lin, E. Rogers, P. Grunmann, V. Koren, G. Gayno, and J. D. Tarpley (2003), Implementation of Noah land surface model advances in the National Centers for Environmental Prediction operational mesoscale Eta model, *J. Geophys. Res.*, *108*(D22), 8851, doi:10.1029/2002JD003296.

England, D. E., and R. T. McNider (1995), Stability functions based upon shear functions, *Boundary Layer Meteorol.*, *74*, 113–130, doi:10.1007/BF00715713.

Esau, I. (2008), Formulation of the planetary boundary layer feedback in the Earth's climate system, *Comput. Technol.*, *13*, 95–103.

Friedman, M., and W. Qiu (2008), On the location and continuation of Hopf bifurcations in large-scale problems, *Int. J. Bifurcat. Chaos Appl. Sci. Eng.*, *18*(5), 1589–1597, doi:10.1142/S0218127408021208.

Fu, Q., and K. N. Liou (1993), Parameterization of the radiative properties of cirrus clouds, *J. Atmos. Sci.*, *50*, 2008–2025, doi:10.1175/1520-0469(1993)050<2008:POTRPO>2.0.CO;2.

Garratt, J. R., and R. A. Brost (1981), Radiative cooling effects within and above the nocturnal boundary layer, *J. Atmos. Sci.*, *38*, 2730–2746, doi:10.1175/1520-0469(1981)038<2730:RCEWAA>2.0.CO;2.

Hansen, J., R. Ruedy, J. Glascoe, and M. Sato (1999), GISS analysis of surface temperature change, *J. Geophys. Res.*, *104*, 30,997–31,022, doi:10.1029/1999JD900835.

Holtslag, A. A. M. (2006), GEWEX Atmospheric Boundary-layer Study (GABLS) on stable boundary layers, *Boundary Layer Meteorol.*, *118*, 243–246, doi:10.1007/s10546-005-9008-6.

Holtslag, A. A. M., and B. A. Boville (1993), Local versus nonlocal boundary-layer diffusion in a global climate model, *J. Clim.*, *6*, 1825–1842, doi:10.1175/1520-0442(1993)006<1825:LVNBLD>2.0.CO;2.

Holtslag, A. A. M., G. J. Steeneveld, and B. J. H. van de Wiel (2007), Role of land-surface temperature feedback on model performance for the stable boundary layer, *Boundary Layer Meteorol.*, *125*, 361–376, doi:10.1007/s10546-007-9214-5.

Jacobson, M. Z. (1997), Development and application of a new air pollution modeling system–Part III. Aerosol-phase simulations, *Atmos. Environ.*, *31*, 587–608, doi:10.1016/S1352-2310(96)00201-4.

Johnson, G. T., T. R. Oke, T. J. Lyons, D. G. Steyn, I. D. Watson, and J. A. Voogt (1991), Simulation of surface urban heat islands under "ideal" conditions at night. Part 1: Theory and tests against field data, *Boundary Layer Meteorol.*, *56*, 275–294, doi:10.1007/BF00120424.

Karl, T. R., P. D. Jones, R. W. Knight, G. Kukla, N. Plummer, V. Razvayev, K. P. Gallo, J. Lindseay, R. J. Charlson, and T. C. Peterson (1993), Asymmetric trends in surface temperature, *Bull. Am. Meteorol. Soc.*, *74*, 1007–1023, doi:10.1175/1520-0477(1993)074<1007:ANPORG>2.0.CO;2.

Kiehl, J. T. (2007), Twentieth century climate model response and climate sensitivity, *Geophys. Res. Lett.*, *34*, L22710, doi:10.1029/2007GL031383.

Kosović, B., and J. A. Curry (2000), A large eddy simulation study of a quasi-steady, stably stratified atmospheric boundary layer, *J. Atmos. Sci.*, *57*, 1052–1068, doi:10.1175/1520-0469(2000)057<1052:ALESSO>2.0.CO;2.

Lorenz, E. N. (1995), Predictability: A problem partly solved, in *Predictability of Weather and Climate, 2006*, edited by T. Palmer, pp. 40–58, Cambridge Univ. Press, Cambridge, U. K.

Louis, J. F. (1979), A parametric model of vertical eddy fluxes in the atmosphere, *Boundary Layer Meteorol.*, *17*, 187–202, doi:10.1007/BF00117978.

Lubin, D., S. K. Satheesh, G. McFarquar, and A. J. Heymsfield (2002), Longwave radiative forcing of Indian Ocean tropospheric aerosol, *J. Geophys. Res.*, *107*(D19), 8004, doi:10.1029/2001JD001183.

Mackaro, S., R. McNider, and A. Pour Biazar (2011), Some physical and computational issues in land surface data assimilation of satellite skin temperatures, *Pure Appl. Geophys.*, *169*, 401–414, doi:10.1007/s00024-011-0377-0.

Mahrt, L. (1987), Grid averaged fluxes, *Mon. Weather Rev.*, *115*, 1550–1560, doi:10.1175/1520-0493(1987)115<1550:GASF>2.0.CO;2.

Mahrt, L. (1999), Stratified atmospheric boundary layers, *Boundary Layer Meteorol.*, *90*, 375–396, doi:10.1023/A:1001765727956.

McNider, R. T., and R. A. Pielke (1981), Diurnal boundary layer development over sloping terrain, *J. Atmos. Sci.*, *38*, 2198–2212, doi:10.1175/1520-0469(1981)038<2198:DBLDOS>2.0.CO;2.

McNider, R. T., A. J. Song, D. M. Casey, P. J. Wetzel, W. L. Crosson, and R. M. Rabin (1994), Toward a dynamic-t thermodynamic assimilation of satellite surface temperature in numerical atmospheric models, *Mon. Weather Rev.*, *122*, 2784–2803, doi:10.1175/1520-0493(1994)122<2784:TADTAO>2.0.CO;2.

McNider, R. T., X. Shi, M. Friedman, and D. E. England (1995), On the predictability of the stable atmospheric boundary layer, *J. Atmos. Sci.*, *52*, 1602–1614, doi:10.1175/1520-0469(1995)052<1602:POTSAB>2.0.CO;2.

McNider, R. T., W. M. Lapenta, A. Biazar, G. Jedlovec, R. Suggs, and J. Pleim (2005), Retrieval of grid scale heat capacity using geostationary satellite products: Part I: Case-study application, *J. Appl. Meteorol.*, *44*, 1346–1360, doi:10.1175/JAM2270.1.

Meehl, G. A., C. Covey, T. Delworth, M. Latif, B. McAvaney, J. F. B. Mitchell, R. J. Stouffer, and K. E. Taylor (2007), The WCRP CMIP3 multi-model dataset: A new era in climate change research, *Bull. Am. Meteorol. Soc.*, *88*, 1383–1394, doi:10.1175/BAMS-88-9-1383.

Nair, U. S., R. McNider, F. Patadia, S. A. Christopher, and K. Fuller (2011), Sensitivity of nocturnal boundary layer temperature to tropospheric aerosol surface radiative forcing under clear-sky conditions, *J. Geophys. Res.*, *116*, D02205, doi:10.1029/2010JD014068.

Parker, D. E. (2004), Large-scale warming is not urban, *Nature*, *432*, 290, doi:10.1038/432290a.

Parker, D. E. (2006), A demonstration that large-scale warming is not urban, *J. Clim.*, *19*, 2882–2895, doi:10.1175/JCLI3730.1.

Peterson, T. C., and R. S. Vose (1997), An overview of the Global Historical Climatology Network temperature database, *Bull. Am. Meteorol. Soc.*, *78*, 2837–2849, doi:10.1175/1520-0477(1997)078<2837:AOOTGH>2.0.CO;2.

Pielke, R. A., Sr. (1984), *Mesoscale Meteorological Modeling*, 1st ed., 612 pp., Academic, San Diego, Calif.

Pielke, R. A., Sr., and Y. Mahrer (1975), Representation of the heated-planetary boundary layer in mesoscale models with coarse vertical resolution, *J. Atmos. Sci.*, *32*, 2288–2308, doi:10.1175/1520-0469(1975)032<2288:ROTHPB>2.0.CO;2.

Pielke, R. A., Sr., and T. Matsui (2005), Should light wind and windy nights have the same temperature trends at individual levels even if the boundary layer heat content is the same?, *Geophys. Res. Lett.*, *32*, L21813, doi:10.1029/2005GL024407.

Pielke, R. A., Sr., et al. (2007), Unresolved issues with the assessment of multi-decadal global land temperature trends, *J. Geophys. Res.*, *112*, D24S08, doi:10.1029/2006JD008229.

Poulos, G., et al. (2002), CASES−99: A comprehensive investigation of the stable boundary layer, *Bull. Am. Meteorol. Soc.*, *83*(4), 555–581, doi:10.1175/1520-0477(2002)083<0555:CACIOT>2.3.CO;2.

ReVelle, D. O. (1993), Chaos and "bursting" in the planetary boundary layer, *J. Appl. Meteorol.*, *32*, 1169–1180, doi:10.1175/1520-0450(1993)032<1169:CAITPB>2.0.CO;2.

Seydel, R. (1988), *From Equilibrium to Chaos: Practical Bifurcation and Stability Analysis*, 367 pp., Elsevier, New York.

Shi, X. (1997), Numerical investigation of the stable nocturnal boundary layer, PhD dissertation, Dep. of Math. Sci., Univ. of Ala. in Huntsville, Huntsville.

Shi, X., R. T. McNider, D. E. England, M. J. Friedman, W. Lapenta, and W. B. Norris (2005), On the behavior of the stable boundary layer and role of initial conditions, *Pure Appl. Geophys.*, *162*, 1811–1829, doi:10.1007/s00024-005-2694-7.

Staley, D. O., and G. M. Jurica (1972), Effective atmospheric emissivity under clear skies, *J. Appl. Meteorol.*, *11*, 349–356, doi:10.1175/1520-0450(1972)011<0349:EAEUCS>2.0.CO;2.

Steeneveld, G. J., B. J. H. van de Wiel, and A. A. M. Holtslag (2006), Modeling the evolution of the atmospheric boundary layer coupled to the land surface for three contrasting nights in CASES-99, *J. Atmos. Sci.*, *63*, 920–935, doi:10.1175/JAS3654.1.

Steeneveld, G. J., T. Mauritsen, E. I. F. de Bruijn, J. Vila-Guerau de Arellano, G. Svensson, and A. A. M. Holtslag (2008a), Evaluation of limited area models for the representation of the diurnal cycle and contrasting nights in CASES99, *J. Appl. Meteorol. Climatol.*, *47*, 869–887, doi:10.1175/2007JAMC1702.1.

Steeneveld, G. J., A. A. M. Holtslag, C. J. Nappo, B. J. H. van de Wiel, and L. Mahrt (2008b), Exploring the possible role of small scale terrain drag on stable boundary layers over land, *J. Appl. Meteorol. Climatol.*, *47*, 2518–2530, doi:10.1175/2008JAMC1816.1.

Steeneveld, G. J., M. J. J. Wokke, C. D. Groot Zwaaftink, S. Pijlman, B. G. Heusinkveld, A. F. G. Jacobs, and A. A. M. Holtslag (2010), Observations of the radiation divergence in the surface layer and its implication for its parameterization in numerical weather prediction models, *J. Geophys. Res.*, *115*, D06107, doi:10.1029/2009JD013074.

Steeneveld, G. J., A. A. M. Holtslag, R. T. McNider, and R. A. Pielke Sr. (2011), Screen level temperature increase due to higher atmospheric carbon dioxide in calm and windy nights revisited, *J. Geophys. Res.*, *116*, D02122, doi:10.1029/2010JD014612.

Stone, D. A., and A. J. Weaver (2003), Factors contributing to diurnal temperature range trends in the twentieth and twenty first century simulations of the CCAma coupled model, *Clim. Dyn.*, *20*, 435–445.

Stull, R. B. (1983), A heat-flux history length scale for the nocturnal boundary layer, *Tellus, Ser. A*, *35*, 219–230, doi:10.1111/j.1600-0870.1983.tb00199.x.

Stull, R. B. (1988), *An Introduction to Boundary Layer Meteorology*, Kluwer Acad., Norwell, Mass.

Sun, J., and L. Mahrt (1995), Determination of surface fluxes from the surface radiative temperature, *J. Atmos. Sci.*, *52*, 1096–1106, doi:10.1175/1520-0469(1995)052<1096:DOSFFT>2.0.CO;2.

Taylor, P. A. (1971), Airflow above changes in surface heat flux, temperature and roughness; an extension to include the stable case, *Boundary Layer Meteorol.*, *1*(4), 474–497, doi:10.1007/BF00184785.

Travis, D. J., A. Carleton, and R. Lauritsen (2004), Regional variations in U.S. diurnal temperature range for the 11–14 September 2001 aircraft groundings: Evidence of jet contrail influence on climate, *J. Clim.*, *17*, 1123–1134, doi:10.1175/1520-0442(2004)017<1123:RVIUDT>2.0.CO;2.

van der Velde, I. R., G. J. Steeneveld, B. G. J. Wichers Schreur, and A. A. M. Holtslag (2010), Modeling and forecasting the onset and duration of severe radiation fog under frost conditions, *Mon. Weather Rev.*, *138*, 4237–4253, doi:10.1175/2010MWR3427.1.

Van de Wiel, B. J. H., R. J. Ronda, A. F. Moene, H. A. R. De Bruin, and A. A. M. Holtslag (2002a), Intermittent turbulence and oscillations in the stable boundary layer over land. Part I: A bulk model, *J. Atmos. Sci.*, *59*, 942–958, doi:10.1175/1520-0469(2002)059<0942:ITAOIT>2.0.CO;2.

Van de Wiel, B. J. H., A. F. Moene, R. J. Ronda, H. A. R. De Bruin, and A. A. M. Holtslag (2002b), Intermittent turbulence and oscillations in the stable boundary layer over land. Part II. A system dynamics approach, *J. Atmos. Sci.*, *59*, 2567–2581, doi:10.1175/1520-0469(2002)059<2567:ITAOIT>2.0.CO;2.

Van Ulden, A. P., and A. A. M. Holtslag (1985), Estimation of atmospheric boundary layer parameters for diffusion applications, *J. Clim. Appl. Meteorol.*, *24*, 1196–1207, doi:10.1175/1520-0450(1985)024<1196:EOABLP>2.0.CO;2.

Viterbo, P., and A. C. M. Beljaars (1995), An improved land surface parameterization scheme in the ECMWF model and its validation, *J. Clim.*, *8*, 2716–2748, doi:10.1175/1520-0442(1995)008<2716:AILSPS>2.0.CO;2.

Viterbo, P., A. Beljaars, J. F. Mauhoff, and J. Teixeira (1999), The representation of soil moisture freezing and its impact on the SBL, *Q. J. R. Meteorol. Soc.*, *125*, 2401–2426, doi:10.1002/qj.49712555904.

Vogelezang, D. H. P., and A. A. M. Holtslag (1996), Evaluation and model impacts of alternative boundary-layer height formulations, *Boundary Layer Meteorol.*, *81*, 245–269, doi:10.1007/BF02430331.

Vose, R. S., D. R. Easterling, and B. Gleason (2005), Maximum and minimum temperature trends for the globe: An update through 2004, *Geophys. Res. Lett.*, *32*, L23822, doi:10.1029/2005GL024379.

Walters, J. T., R. T. McNider, X. Shi, and W. B. Norris (2007), Positive surface temperature feedback in the stable nocturnal boundary layer, *Geophys. Res. Lett.*, *34*, L12709, doi:10.1029/2007GL029505.

Wang, J., and S. A. Christopher (2006), Mesoscale modeling of Central American smoke transport to the United States: 2. Smoke radiative impact on regional surface energy budget and boundary layer evolution, *J. Geophys. Res.*, *111*, D14S92, doi:10.1029/2005JD006720.

Wang, J., S. A. Christopher, U. S. Nair, J. S. Reid, E. M. Prins, J. Szaykman, and J. L. Hand (2006), Mesoscale modeling of Central American smoke transport to the United States: 1. "Top-down" assessment of emission strength and diurnal variation impacts, *J. Geophys. Res.*, *111*, D05S17, doi:10.1029/2005JD006416.

Weil, J. C. (2011), Stable boundary layer modeling for air quality applications, in *Air Pollution Modeling and Its Application XXI*, edited by S. T. Castelli and D. Steyn, pp. 57–61, Springer, New York, doi:10.1007/978-94-007-1359-8_10.

Zhou, L., R. E. Dickinson, A. Dai, and P. Dirmeyer (2010), Detection and attribution of anthropogenic forcing to diurnal temperature range changes from 1950 to 1999: Comparing multi-model simulations with observations, *Clim. Dyn.*, *35*, 1289–1307, doi:10.1007/s00382-009-0644-2.

Zilitinkevich, S. S. (1970), *Dynamics of the Atmospheric Boundary Layer*, 291 pp., Leningrad Gidrometeor, Leningrad, Russia.